Implementation of Robust Fractional-Order Neural Modified Sliding Mode Controls for Managing the Power Output of Doubly Fed Induction Generators

Habib Benbouhenni*‡, Nicu Bizon**

*LAAS laboratory, National Polytechnic School of Oran-Maurice Audin, BP 1523 Oran El M'naouer, Algeria

**The National University of Science and Technology Politehnica Bucharest, Pitești University Centre, 110040 Pitesti, Romania

(habib.benbouhenni@enp-oran.dz, nicu.bizon1402@upb.ro)

‡Corresponding Author; Habib Benbouhenni,BP 1523 Oran El M'naouer,Tel: +213663956329,

habib.benbouhenni@enp-oran.dz

Received: 12.10.2025 Accepted: 02.12.2025

Abstract-This paper presents a robust fractional-order neural-modified sliding mode control (FONMSMC) strategy for enhancing the performance of dual-rotor wind turbines (DRWTs) driven by doubly-fed induction generators (DFIGs). Conventional direct power control methods often exhibit unstable power output, high electrical noise, and limited adaptability under variable wind conditions. The proposed FONMSMC integrates fractional calculus for precise dynamic tuning, neural networks for adaptive adjustment, and a modified sliding mode control framework to improve robustness, combined with pulse-width modulation for efficient power conversion. Simulation results demonstrate significant performance improvements, including reductions of up to 94% in active power steady-state error, 87.2% in active power fluctuations, and 71.79% in total harmonic distortion. The controller also maintains stable operation across a wide range of wind speeds, ensuring enhanced grid stability and reduced mechanical stress. The proposed method offers a reliable and efficient control solution for DFIG-based DRWT systems, contributing to improved sustainability and robustness in modern wind energy applications.

Keywords: Dual-rotor wind turbine systems, fractional-order neural modified sliding mode approach, direct power control, neural networks, doubly-fed induction generators.

1. Introduction

The increasing power demand has spurred the search for alternative, high-efficiency energy solutions. The incorporation of renewable power sources (RPSs), such as wind energy (WE) systems, into energy networks presents new challenges in enhancing power quality (PQ) and production. In [1], a wind turbine (WT) generator was combined with photovoltaic (PV) cells, a power storage system (PSS), a fuel cell (FC), and an electrolyzer to generate energy. This proposed energy system (ES) is capable of producing energy under various challenging weather conditions. Within this proposed ES, a priority-based load-shedding method was developed to maintain effective energy coordination between different RPSs and storage devices. This strategy enables the ES to operate reliably in both standalone and extended operation modes. Results explained the competence of this algorithm in enhancing the dynamic response (DR) of the studied ES. Additionally, the results highlight the successful integration of the various components in the power generation process, underscoring the significant potential of this system for the future.

However, this ES has the drawback of being complex and difficult to control. As is well-known, WE is characterized by volatility and randomness, which can lead to unstable energy output, ultimately resulting in inefficiencies within the ES. In [2], an adaptive offloading scheme is introduced to enhance the output power of a variable-speed WT generator. The

discharge process of the WT generator creates reserve energy at maximum power point (MPP) operation. This reserve can be utilized to stabilize frequency variations in the ES during emergencies, making the proposed method highly significant for the energy sector.

During ES events, the output energy of the vacuum WT generator is dynamically controlled to improve the fundamental frequency response. The nonlinear energy feature curve of the WT is processed using the Lagrange Interpolating Polynomial, which helps increase the output energy of the unloaded WT generator. Additionally, the LIP-based unloading of the WT generator enhances dynamic frequency performance during various ES scenarios, such as variations in wind speed (WS) and variations in load, compared to conventional methods in the ES. The suggested method is applied using real-time hardware-in-the-loop (HIL) simulation. The results demonstrate the efficiency of this algorithm in enhancing the operational characteristics of the WT generator. The author of [3] argues that integrating RPSs, such as PV solar cells and WTs, into direct current (DC) microgrids (DCMs) presents significant challenges, particularly for applications like DC fast charging of electric vehicles. These challenges include low inertia, power fluctuations, and voltage instability. To address these issues, a hybrid approach combining the firefly and particle swarm optimization (FA-PSO) algorithm was employed to fine-tune the neuro-fuzzy (NF) technique, Takagi-Sugeno fuzzy inference systems, and fractional-order proportional-integral-derivative (FO-PID) regulators used for power management within the DCM. This proposed method ensures faster convergence, improved accuracy, and fewer topological constraints. A comprehensive small signal stability analysis was performed to evaluate the impact of the hybrid optimization techniques on the DCM's stability. MATLAB was utilized to validate these strategies under real-world uncertainties, such as fluctuations in WS and sunlight exposure. The results demonstrated the effectiveness and practicality of these methods for DCMs that incorporate integrated charging solutions for electric vehicles.

In recent years, large-scale WE conversion systems (WECSs) that utilize doubly-fed induction generators (DFIGs) have gained significant popularity due to their numerous economic and technical advantages [4]. As the integration of WE into the power grid continues to grow, DFIG-based WECSs need to remain connected during grid fault scenarios and provide the necessary reactive power (*Qs*) to the grid. However, the direct connection of the DFIG's stator to the grid makes it vulnerable to grid disturbances, particularly voltage drops. To address this issue, a modified demagnetization method is designed to enhance the low-voltage ride-through (LVRT) capability of DFIGs during grid faults. This algorithm is realized in a coordinated manner, utilizing demagnetization current control and incorporating an external resistance at the rotor-side converter (RSC) of the DFIG. The demagnetization control ES reduces the DC component of the flux, while the external resistance speeds up the damping of the transient flux by lowering the time constant. This improvement strengthens the LVRT capability of the DFIG. The competence of the designed algorithm was validated through simulations in MATLAB, examining both symmetric and asymmetric network faults. The results, along with comparisons made, demonstrate the advantages of this methodology in enhancing the performance of the studied ESs.

The motivation for this study arises from the necessity of developing a robust controller that effectively addresses issues related to PQ and current quality, while also significantly enhancing system robustness. By improving the competence, efficacy, and reliability of ESs, this research aims to tackle the challenges posed by low power quality and high total harmonic distortion (THD) of current in WECSs.

In the energy field, electric power generation is considered one of the most prominent topics of the era due to its social and economic importance to the governments of countries. The trend towards RPSs is the most eminent option available now, which has shown acceptable performance in power generation, as it can be relied upon for energy supply [5]. The utilization of these energy sources represents a promising strategy for governments seeking to reduce dependence on petroleum-based resources. The most prominent of these solutions, which have gained widespread popularity on land and at sea, are WTs [6]. These WTs are divided into two kinds: horizontal-axis WTs [7] and vertical-axis WTs [8]. According to the work done in [9], horizontal-axes WTs are the most widespread and used throughout the world on land and at sea. But the power supply of WT systems based on grid-connected DFIGs faces major challenges during grid failure. As is known, disturbances generated from the network greatly affect the operation of DFIGs [10]. In addition, controlling powers are one of the most prominent priorities that must be given great attention and importance. The control method is primarily responsible for PQ and good operation. Choosing a control strategy with high features gives high performance to the ES.

Several research studies have proposed algorithms to enhance the efficacy and robustness of DFIG-based WT systems [11-15]. These proposed control schemes can be categorized into four main sections: linear control algorithms, smart control schemes, nonlinear control schemes, and hybrid control algorithms.

Nonlinear algorithms include sliding mode control (SMC) [16], terminal SMC [17], high-order SMC strategies [18], backstepping control (BC) [19], synergetic control (SC) [20], and terminal SC techniques [21]. These techniques offer robustness features compared to conventional algorithms such as direct torque control (DTC) and field-oriented control (FOC). However, they are often complex to implement, particularly SMC and BC, which are associated with the studied ESs. This complexity makes it challenging to apply these nonlinear methods to intricate ESs, such as 7-phase motor control.

Smart techniques refer to approaches that utilize artificial intelligence, such as fuzzy logic (FL) [22] and neural algorithms (NAs) [23]. These techniques are well-known for their accuracy and quick response times (RTs). Unlike traditional methods, smart controls do not rely on fixed mathematical rules or relationships for their application in

embedded systems. Instead, they depend significantly on the experience and intelligence of the user.

When compared to nonlinear strategies, smart controls provide a superior solution for regulating machines. It is widely recognized that adopting a smart approach enhances control methods and minimizes undulations in generated currents, magnetic flux, and torque in machines. Furthermore, the implementation of intelligent control strengthens the robustness of control schemes.

Hybrid control strategies (HCSs) are techniques that combine the strengths of nonlinear methods with advanced technologies to create more robust and accurate controllers. HCSs aim to enhance the features of traditional approaches, improve the efficiency of electrical machines, and reduce ripples in both the torque and current of these machines. These strategies have demonstrated significant success in decreasing ripple effects and enhancing the DR of electric machines compared to using only smart techniques or nonlinear strategies. Consequently, HCSs offer an effective solution for regulating machines, helping to reduce the frequency and costs of periodic maintenance while also extending the overall lifespan of the system.

One notable application of this approach is the integration of the BC technique with intelligent control based on a Genetic Algorithm (GA) to manage the DFIG energy [24]. The results indicate that this designed approach exhibits highly favorable characteristics. In [25], the SMC technique and NAs are combined to minimize the ripples in the generated active power (*Ps*) and *Qs* of the DFIG. The NA-SMC strategy is described as highly competent and strength. This strategy significantly improves DR and PQ, as demonstrated by simulation results across all conducted tests. However, the NN-SMC technique has some disadvantages; it is impacted by changes in DFIG parameters due to its reliance on the mathematical model (MM) of the ES. Additionally, using the NA-SMC to control power requires power estimation, which is also related to the DFIG parameters. This reliance increases the vulnerability to changes in those parameters. In [26], the author implemented fractional-order super-twisting sliding mode control (FOSTSMC) to enhance the supercapacitor control scheme for managing the power of the DFIG. This control strategy aims to enhance PQ and protect the DFIG. One of the key advantages of using fractional calculus is that it does not require data on the modeling parameters of the ESS, making its application straightforward. The developed supercapacitor technique demonstrates exceptional capabilities and high robustness, independent of the ESSs modeling parameters, unlike other strategies. This approach was compared with FL techniques, standard SMC, and proportional-integral (PI) regulators, with MATLAB used to validate the proposed control method. The results indicate that the novel supercapacitor algorithm significantly enhances the stability of the ESS compared to the other methods. Additionally, the suggested technique reduces the current THD when compared to both the FL technique and PI control. It also minimizes power ripples, which is a positive indicator of the efficiency and competence of this control method. However, this approach does come with some drawbacks, including its complexity and the need for power estimation, which can make implementation challenging and potentially increase costs. In the study [27], a fractional calculus strategy was applied to a proportional-integral-derivative (PID) regulator to enhance the fineness of energy generated by the DFIG. The control parameters were determined using the Grey Wolf Optimization (GWO), which improved the competence and strength of the proposed control system. This approach is recognized for its high effectiveness and robustness against variations in DFIG parameters. MATLAB was used to validate the efficacy and capability of the new method. The results indicate that this approach significantly minimizes energy fluctuations and the current THD compared to PID methods. However, despite the strong efficacy of the new algorithm, the issue of energy fluctuations remains due to the use of a modulation method in the DFIG.

Conversely, the modulated unified PQ controller (M-UPQC) is suggested in [28] to enhance the PQ components in small AC networks. This controller operates based on the principles of current and voltage source converters and the resonant component of the ES. The Black Hole Optimization (BHO) and Particle Swarm Optimization (PSO) are utilized to determine the gain values of the proposed controller, thus improving performance and reducing THDs in the ES. Simulation results demonstrate improved operation of the AC grid with the designed algorithm when compared to usual methods. Furthermore, experimental results confirm the competence of the new algorithm in enhancing the power quality characteristics of the small AC grid and in minimizing the current THD. The author in [29] discusses the significance of Hydrogen ESSs and battery ESSs in renewable energy-based ESs, highlighting their role in providing efficient energy storage and ensuring PQ. He emphasizes that enhancing PQ, particularly in terms of voltage stability and THD minimization, is a key advantage of both hydrogen-based ESs and battery ESS. To address this, the author proposes a novel approach known as the Dual d-q (DDQ) strategy aimed at improving the performance and power/current quality of hybrid ESSs. This DDQ approach is compared with traditional methods, including PI control and decoupled d-q (DEDQ) control strategies. Simulation results demonstrate the effectiveness and superiority of the DDQ approach, achieving an efficiency of 98%, compared to 81% for the DEDQ method and just 12% for the PI. Furthermore, the DDQ approach shows significant effectiveness in managing energy flow and maintaining high PQ in integrated hydrogen systems and battery ESS, outpacing conventional control methods. This positions it as a promising strategy for future hybrid ESSs.

The optimal robust disturbance observer-based SMC (RDO-SMC) technique was developed to enhance the effectiveness of the ESS [30]. This method employs a multi-objective grasshopper optimization (MOGO) to determine the gain values for the designed RDO-SMC. It has shown notable and effective performance in enhancing the stability of the ES. Key features of this control method include its simplicity and ease of application. The proposed RDO-SMC was tested in MATLAB, and the results indicated a faster DR compared to conventional approaches. However, the RDO-SMC strategy has some drawbacks; a significant limitation is its dependence on the models of the ES. This reliance can lead to

unsatisfactory results if there are changes in the ES parameters. In a related study [31], a robust perturbation observer-based fractional-order SMC (RPO-FOSMC) was utilized to manage the energy output of the DFIG. This approach aimed to enhance the fault ride-through (FRT) capability and enhance MPP tracking (MPPT). Additionally, the MOGO was used to raise the strength and effectiveness of the RPO-FOSMC technique. The proposed method was validated through extensive testing in MATLAB, allowing for a comparison of its performance against conventional control strategies. The results demonstrated that the RPO-FOSMC exhibited exceptional disturbance rejection capability when compared to traditional control methods. Moreover, this approach significantly improved PQ, which is a positive outcome. However, the complexity of this control method presents a drawback, making it costly to implement experimentally. Furthermore, the model-based approach for the ESS can lead to a decline in power and current fineness if the parameters of the ES change.

In [32], a hierarchical deep learning-based recurrent convolutional NN (HDL-RCNN) was introduced to enhance the characteristics of microgrids, specifically regarding the precise regulation of voltage and frequency (V/F) components and improving PQ. This strategy offers significant numerical advantages, such as high strength and excellent operational performance. The results show notable improvements in V/F control: in Network 1, voltage ripples decreased from 0.028 pu to 0.004 pu, while frequency fluctuations in Network 2 reduced from 0.025 pu to 0.007 pu. Furthermore, the approach ensures voltage stability at a level of 1 unit, with minimal ripples, and demonstrates robust performance under dynamic load changes and noisy conditions. In [33], a finite-time control scheme (FTCS) is introduced for managing pulse width modulation (PWM) in microgrid systems. This approach aims to enhance V/F regulation within a defined time frame while also reducing power ripples compared to conventional strategies. By incorporating FTCS into a low-power regulator, the ES achieves fast and accurate regulation that outperforms usual algorithms. A comparative analysis with the SMC strategy demonstrates the superior performance of FTCS, especially in isolated island configurations. MATLAB simulations conducted across three microgrid scenarios show significant ameliorations in key metrics, including voltage and energy ripples, load current ripples, and *Ps*/*Qs* outputs. The results indicate a 50% reduction in voltage drop in PV modules, an 8% increase in *Ps* output, and a 90% minimization in frequency deviations, highlighting the efficacy of the FTCS system. These findings confirm that the FTCS system enhances overall performance, providing a more reliable and flexible solution for managing the obstacles associated with integrating RESs into smart ESs. A comparison conducted in [34] demonstrates the effectiveness and advantages of the SMC in enhancing the features of the FOC for DFIG. The SMC was assessed against PI regulators in terms of performance and efficacy in enhancing PQ and DR. Traditional PI regulators exhibit several limitations due to the nonlinear nature of the DFIG model, highlighting the need for alternative solutions. The SMC approach offers significant improvements in both performance and durability compared to conventional controllers. Results indicate that the proposed algorithm effectively diminutive power undulations, overshoot, and THD in the current when compared to PI control. However, the SMC method does have some drawbacks, including sensitivity to variations in DFIG parameters and the occurrence of the chattering phenomenon, which can lead to undesirable effects.

A new regulator for the RSC drive control of a DFIG-based dual-rotor WT (DRWT) was proposed in [35]. This control strategy combines fractional calculus with an NA method. It is described by its simplicity, high efficiency, and low charges, making it a suitable choice for this application. The design of this control system is informed by practical experience with NA algorithms. It regulates energy by determining voltage reference values (VRVs) based on energy errors. A PWM is then employed to convert these VRVs into pulses that operate the RSC. The proposed control system demonstrates significant effectiveness in handling fluctuations, steady-state error (SEE), and THD values. Furthermore, it has shown satisfactory results regarding RT, minimization of fluctuations, and THD when compared to other research efforts. However, despite its impressive performance, this control method has some drawbacks. Notably, it lacks established rules to simplify the application of the NA method and relies heavily on power estimation.

The author in [36] argues that the fractional-order FL approach is one of the most effective methods for regulating DFIG, thanks to its high robustness and exceptional performance. This approach offers several advantages, including independence from the mathematical modeling of the ES, simplicity, ease of realization, and quick DR. This method was applied to control the RSC by generating VRVs as part of the designed control ES. These VRVs were then used to estimate the pulse values necessary for operating the RSC, utilizing the PWM. The efficacy of the fractional-order FL was verified using MATLAB, and its results were compared to both DPC and findings from various research works, with two distinct WS profiles considered. The results showed that the fractional-order FL method outperformed the DPC method, particularly regarding RT and THD. However, there are some limitations to this approach, including the presence of ambiguous control rules and a reliance on energy estimation. This dependence ties the method to the parameters of the ES, which can help mitigate current and energy ripples during faults within the ES.

In [37], the author employed a fractional-order SC method as an effective solution for power control in DFIG. This control method utilizes VRVs as its output. Notable features of this approach include simplicity, high effectiveness, ease of control, and robustness. The study compared a DRWT to a conventional WT in terms of power generation from WE and rotational speed. The control design was tested in MATLAB under various operating conditions for the DFIG, yielding results that showed significant improvements in power fluctuations, overshoot, current THD, and SSE values. However, a drawback of this approach is its RT, which was found to be unacceptable compared to the DPC. Another nonlinear control method suggested for energy management in [38] combines fractional calculus, the sliding control approach, and a PI regulator. To calculate the gains for this

designed control, the PSO algorithm was utilized. As a result, high robustness, efficiency, and distinguished competence are significant features of this designed method. This approach yielded suitable results in robustness testing, indicating its ability to enhance ES features in the presence of faults, which is positive. However, the drawbacks of this technique include its reliance on energy estimation, which explains the noticeable increase in ripple values, overshoot, SSE, and THD values.

The NN-SC-STC technique was developed to address the shortcomings of the DPC [39]. This method combines the strengths of NA algorithms, the simplicity and robustness of the SC, and the high performance of STC. It was applied to a system designed to determine VRVs based on the power line. The MPPT was used to estimate the power reference (Ps^*). While this approach has some drawbacks related to the selection of NA properties necessary for achieving high efficiency, the results indicate that it offers significant improvements despite these challenges. Notably, the use of this method has led to reductions in ripple, overshoot, current THD, and SSE.

In another study [40], the disadvantages of the DPC strategy were examined further, with the author highlighting that ripples, lack of robustness, and excessive THD are among the main issues with this approach. As a solution, the author recommended using an intelligent STC strategy, which is highly effective and competent. This is supported by test results, demonstrating significant enhancements in THD and PQ compared to both the DPC and other research. Furthermore, this innovative approach was implemented in an HIL test, where the empirical results confirmed the accuracy of the simulations and showcased the new approach's effectiveness in enhancing ES features compared to the DPC.

A new approach utilizing a fractional-order STC technique based on the PSO has been proposed [41]. This method demonstrated superior results compared to traditional approaches. It combines three different techniques to enhance control performance and address the deficiencies of DPC in DFIG [42]. Specifically, this approach integrates the terminal sliding surface method, GA, and a PI controller. This control strategy is regarded as more robust, high-performing, and straightforward to implement. It was applied to power control, utilizing a PWM to operate the RSC. Results indicate that this new approach significantly improves ESS features when compared to the DPC. Additionally, another study employed an SC-PI based on the GA to overcome the limitations of the DPC [43]. This algorithm was specifically applied to the RSC, with the PWM used in conjunction. The suggested strategy is described by high efficacy, effectiveness in minimizing fluctuations, and greater robustness when compared to the DPC.

Some researchers have suggested the emergence of two nonlinear strategies to improve control methods. For example, a study combined the SMC with an STC to achieve more robust control while minimizing torque and *Ps* ripples in a DFIG [44]. The results confirmed the robustness of this control design, demonstrating that it remains effective even when the parameters of the DFIG are changed. Additionally, a new hybrid control method has been proposed for managing DFIG-DRWT. This method merges the STC strategy with the SMC technique, showing effectiveness in reducing both power and torque ripples, particularly when tuning the DFIG parameters, in comparison to the DPC method. However, this control has some negatives. The most significant issue is the high number of gains required, making it difficult to adjust the droop response for different energy levels [45]. Furthermore, some power ripples have been observed during robustness testing, which is not desirable.

In reference [46], the author introduced a nonsingular terminal sliding mode surface strategy to enhance the features of the BC strategy, addressing the drawbacks associated with the DPC method. This technique is notable for its high efficiency and effectiveness in mitigating fluctuations and exhibits strong robustness against varying DFIG parameters, outperforming the DPC method. The proposed BC approach calculates VRVs based on energy errors. In this algorithm, PWM is employed to convert the VRVs into operating pulses for the RSC, as accurate power estimation is crucial for the method's implementation. Results demonstrate that this suggested technique provides rapid DR and high robustness compared to several other approaches. Additionally, both PQ and THD of the current improve in all tests when this approach is applied, compared to the DPC. However, there are two significant cons to this algorithm: the number of gains required and its inherent complexity. The complexity can make the suggested method challenging and costly to implement experimentally, which may not be ideal. A different approach was proposed in [47], which utilizes the nonlinear BC method to manage the power of the DFIG-DRWT. This BC method requires precise knowledge of the mathematical model (MM) of the studied ES, linking the control of the ES to the machine's parameters. Additionally, the BC method necessitates power estimation, using the same equations as those found in the DPC. The proposed algorithm was tested in MATLAB under variable WSs. The simulation results indicated that the BC method improved energy fluctuation values, current THD, overshoot, and SSE. However, it did not perform as well as conventional methods regarding RT. During robustness testing, it was observed that the performance of the BC approach was significantly affected by variations in parameters, leading to increased values of RT, energy fluctuations, and current THD. This sensitivity arises from the BC method's reliance on the machine model of the studied ES.

Consequently, it is essential to explore a control technique that does not depend on the generator model. The author of [48] argues that integrating NAs within the STC technique is one of the most effective and reliable solutions for addressing the current issues of THD and PQ when compared to usual methods. To defeat the limitations of the DPC, the use of NAs has significantly increased efficiency and robustness. NAs were chosen for their precision and their ability to operate without a MM of the ES, which greatly enhances both efficiency and energy fineness. The designed approach advances the DPC by utilizing a PWM to run the RSC instead of relying on a switching table (ST). Additionally, an NA-STC technique is employed to manage energy control, replacing

traditional regulators represented by hysteresis comparators (HCs). This new technique is based on energy estimation, which can be affected in the event of a fault within the ES. Results demonstrate a significant impact on robustness during testing. Overall, the proposed approach yielded satisfactory results regarding SSE, ripples, and undershoot when compared to the DPC technique.

Traditionally, WTs are widely accepted as a reliable technology for energy generation due to their advantages over conventional methods, such as gas-based power. This technology is known for reducing greenhouse gas emissions while significantly contributing to the economies of developing countries. WTs convert WE into mechanical power (MP), which is then used to rotate the generator, producing electrical power.

In this work, a different type of WT, known as the DRWT, is selected to enhance the MP generated from WE. This advanced WT design aims to enhance the efficacy of wind farms by increasing the amount of MP converted from WE. The effectiveness of this novel WT technology has been explored in various studies [49-51]. According to the research presented in [52], the implementation of the SMC strategy effectively addressed the issues and defects associated with DPC in DFIG. This improvement is evidenced by the reduced fluctuations in values and the lower THD compared to the DPC. Additionally, employing this algorithm significantly enhanced the robustness of the ES. However, the SMC method also has its drawbacks. Its use markedly increases the complexity of both the strategies and the ESs, making experimental implementation more challenging. The control associated with the MM of the ES can lead to unsatisfactory results if a fault occurs within the system. Such faults may manifest as high ripple values, overshoot, excessive current THD, and poor SSE. In reference [53], the SMC yielded unsatisfactory results compared to the SC method regarding the performance and characteristics of the DFIG-DRWT. To address the shortcomings of the SMC method for the DFIG, the author proposed a new approach called modified SMC (MSMC) in reference [54]. This approach is intended to replace the DPC method in control applications.

The MSMC is described by its simplicity, fewer gain parameters, ease of application, and very fast DR. The MSMC was applied to the direct vector control of the DFIG for power management, producing VRVs which were then converted into pulses to run the RSC using a PWM. Additionally, this approach improved the effectiveness of the MPPT to obtain a reference value for high PQ. The new technique was compared to the SMC using MATLAB under various scenarios involving the DFIG. The test results indicated that the SMC delivered poor internal and numerical outcomes compared to the MSMC, highlighting the benefits of the latter and suggesting its potential as an alternative for future control applications. However, despite the high efficacy of the MSMC, it still encountered challenges related to ripples due to its reliance on energy estimation.

To further enhance PQ, the MSMC was combined with an FL approach in reference [55], resulting in excellent outcomes compared to traditional PI and MSMC. Nonetheless, this combined method also faced challenges due to its dependence on estimation, which introduces some variability.

Recently, various strategies have been employed to manage the power of DFIGs. However, several challenges continue to hinder the widespread adoption of ESs based on RESs, particularly WE. Most of the energy systems proposed in the literature rely on conventional WTs and utilize less efficient control strategies. Many research studies overlook the importance of the turbine in ESs, failing to focus on enhancing the performance and efficiency of WTs.

Traditional WTs often face limitations, such as low power generation in weak wind conditions and vulnerability to damage from strong winds, resulting in increased material losses. These issues impede the adoption and effectiveness of ESs based on WTs, especially in high-wind situations. Furthermore, there is a significant gap in developing a control strategy that is simple to implement, highly robust, and effective at minimizing energy fluctuations while reducing the THD of the current.

Some strategies, including fractional calculus, NN algorithms, and the MSMC technique, have shown remarkable performance in various ESs. The application of the MSMC technique in a DFIG-based ES has demonstrated significant improvements in both robustness and dynamic power responses. However, the performance of the MSMC technique remains inadequate, particularly under conditions with varying parameters.

Driven by these shortcomings, this work introduces an energy system that incorporates a DRWT to maximize energy harvested from the wind. Additionally, a new controller is suggested for the power control of the DFIG. This approach aims to enhance the performance, efficiency, and reliability of the ES while addressing the aforementioned challenges and providing improvements over traditional methods. The competence, efficiency, and strength of the new algorithm are assessed using two distinct wind scenarios and varying parameters of the studied ES. The results are compared to other related works in terms of reducing RT, energy fluctuations, and current THD.

In this study, we introduce a novel controller that combines a feedforward backpropagation neural network—utilizing the conjugate gradient method with Beale-Powell restarts algorithm—fractional-order control, and an MSMC. This robust strategy was specifically designed to control a DFIG-DRWT. The proposed fractional-order neural MSMC (FONMSMC) controller represents a significant contribution of this paper, distinguishing it from prior research.

Key features of the suggested controller include robustness, simplicity, high competence, efficiency, ease of implementation, and independence from the MM of the ES. Although fractional-order control strategies have been explored in various electromechanical and renewable energy systems, their integration with neural network-based slip-mode controllers for DFIG power regulation remains largely unexplored. A comprehensive literature review revealed that no previous studies had applied fractional-order-neural network models to this specific problem. This underscores the

novelty of the proposed neural modified sliding mode controller system (FONMSMC) for managing DFIG power output. For comparison, previous work has implemented neural controllers integrated with fractional control, while other work has focused on SMC controllers integrated with fractional control. The approach designed in this paper uniquely combines both aspects to enhance robustness and adaptability, making the work highly relevant in the field of control and, in particular, in the field of power.

The robust FONMSMC technique was employed to address the limitations of the DPC, and two regulators were utilized to manage the power. Consequently, the robust DPC-FONMSMC is identified as the second major contribution of this paper. This approach has been applied to control the RSC. Additionally, a PWM was used to convert VRVs created by the FONMSMC into pulses for RSC operation.

The robust DPC-FONMSMC is illustrated in the schematic diagram shown in Figure 1. Its characteristics include rapid RT, exceptional robustness, and superior performance compared to the DPC-MSMC. A detailed comparison between the robust DPC-FONMSMC and the DPC-MSMC constitutes the third major contribution of this paper. To implement the new robust algorithm, MATLAB was utilized, employing two different forms of WS to validate the behavior of the new robust algorithm.

The operational performance of the designed approach was also assessed under varying ES parameters and in situations where the MPPT was not applied. A key contribution of this paper is the comparison of the new robust algorithm with the DPC-MSMC. Additionally, this method is evaluated against related works in terms of power undulation minimization, SSE reduction ratios, and current THD. Results underscore the effectiveness of the new robust algorithm in significantly enhancing PQ and current performance compared to the DPC-MSMC.

The following points summarize the objectives achieved by this work:

- Overcoming strategic problems of DPC of DFIG-DRWT.
- Significantly improving PQ compared to some scientific papers.
- Minimizing the current THD compared to the DPC-MSMC and several research studies.
- Significantly raising the strength of the studied ES.
- Significantly improving the overshoot value compared to the DPC-MSMC and several research studies.
- Significantly minimized the SSE value of DFIG energy.

The rest of this study is organized as follows. Section 2 gives an overview of the DRWT. Section 3 includes a detailed overview of the robust FONMSMC suggested in this paper, highlighting the differences between it and the MSMC. In Section 4, the DPC using the robust FONMSMC is presented and compared to the DPC. In Section 5, the simulation results using MATLAB are provided and analyzed. In the final section, there are closing thoughts and essential remarks.

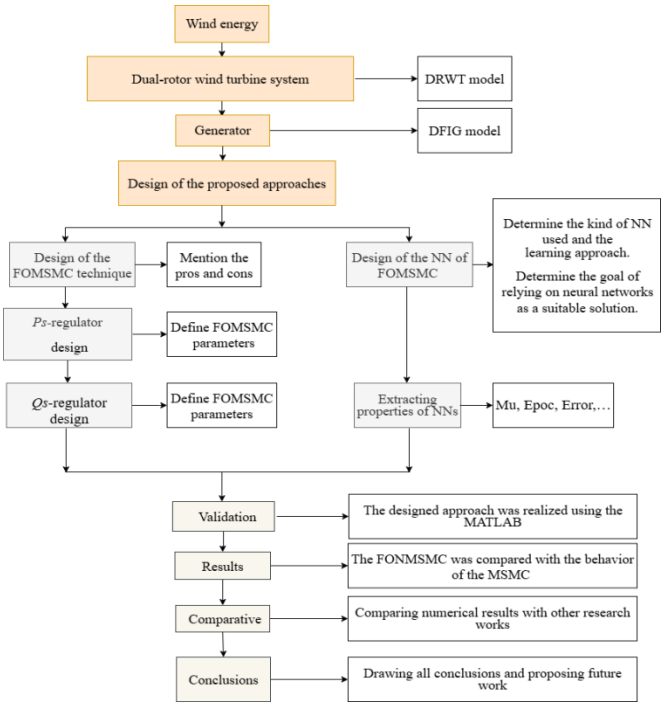

Fig. 1. Diagram for designed method.

2. Turbine Model

Recently, the trend toward renewable energy has increased significantly, especially in developed countries, due to the severity of global warming and the increasing demand for energy. Therefore, WE have been relied upon as an alternative to traditional sources and a suitable and effective solution for generating electricity. WE are among the most widely used energies and one of the most exploited sources in this regard due to its low charges and ease of access [56]. WTs are used to harness WE, generating mechanical energy. As is well known, WE is clean, easy to use, and inexpensive [57]. According to the work done in [58], WTs used to generate electrical energy are classified into vertical-axis WTs and horizontal-axis WTs. Horizontal-axis WTs with three blades are most commonly used. However, these WTs are constantly evolving, with advanced technologies recently emerging to overcome the problems of usual WTs. The author [59] argues that DRWT technology is the most prominent solution proposed to increase the energy yield from WE and to defeat the drawbacks of conventional WTs. Compared to conventional WTs, the use of DRWTs reduces the area of wind farms and defeats the WT overlap between the wind farms, significantly increasing wind farm efficiency and reducing electricity production/consumption costs. Furthermore, the use of DRWTs minimizes the size of the WTs, making them easier to implement on the ground. Furthermore, DRWT turbines are highly resistant to strong winds, allowing for reduced material losses compared to usual WTs. Despite these advantages, DRWT turbines have obstacles, the most significant of which is the presence of a significant number of mechanical components, which require periodic maintenance. DRWT turbines are also more difficult to control than usual WTs and are more expensive.

In general, these WTs are constantly evolving, and their use will enable a technological revolution in the energy sector in the future. Therefore, the use of this WT in this paper is of great importance. Given this significant importance, this WT was used to convert WE into MP. Several works have addressed the mathematical modeling of DRWTs, addressing the challenges that hinder their widespread deployment [60-64]. Figure 2 represents an ES based on a DRWT for generating electrical power. This ES is identified by simplicity, ease of realization, and lower costs. The use of this ES reduces dependence on traditional energy sources, thus protecting the environment from pollution and minimizing the severity of the global warming phenomenon. In this study, a DFIG is used to generate electrical energy due to its ease of control, high robustness, low maintenance, and low cost compared to some generators on the market [65].

In this paper, a two-turbine DRWT, a large-scale WT, and a smaller-scale WT are used to convert WE into MP. The larger-scale WT is used to control the mother WT (DRWT). These WTs rotate in the same direction and are positioned on a single shaft to generate greater torque and power compared to conventional WTs. This type was chosen for its reasonable charges and ease of control compared to some existing multi-rotor WTs. Moreover, the resulting DRWT torque is the sum of the torques of the two WTs [66, 67]. In this WT, several different WTs can be used to form the parent DRWT.

In this paper, two WTs of different power capacities are used to embody the parent DRWT. Therefore, the torque and energy values resulting from DRWT can be expressed by Equation (1).

$$\begin{cases} P_t = P_1 + P_2 \\ T_t = T_1 + T_2 \end{cases} \quad (1)$$

Where, T_1 and T_2 are the torque of both WTs.

T_t and P_t are both torques and energy of the DRWT.

Equation (2) represents the torque of the two WTs [61], where the torque is linked and pertains to the tip speed ratio (TSR) of both WTs (λ_1 and λ_2), the air density (ρ), the blade radius of both WTs ($R_1$and R_2), and the mechanical speed of both WTs (w_1 and w_2).

$$\begin{cases} T_1 = \frac{1}{2\lambda_1^3}.\rho.\pi.R_1^5.C_p.w_1^2 \\ T_2 = \frac{1}{2\lambda_2^3}.\rho.\pi.R_2^5.C_p.w_2^2 \end{cases} \quad (2)$$

The energy output of a DRWT is related to a factor called the coefficient of power (Cp). This coefficient very affects the energy gained from the wind, as its value does not exceed 1. Therefore, the maximum power output, or torque, is achieved when Cp = 1. In the field of WTs, the maximum value of this coefficient is 0.59.

The TSRs λ_1 and the λ_2 of both WTs are shown in Equation (3) [63], where the TSRs are related to both WS (V_1 and V_2) and mechanical speed (w_1 and w_2).

$$\begin{cases} \lambda_1 = \frac{w_1.R_1}{V_1} \\ \lambda_2 = \frac{w_2.R_2}{V_2} \end{cases} \quad (3)$$

There is a difference between the WS before and after the first WT. In addition, the WS between both WTs is distinct from the WS before the first WT. So, the WS before the 2nd WT is represented in Equation (4). The distance (x) between both WTs is 15 meters. The trust coefficient (C_T) and the x between the two WTs are related to the WS between them. This coefficient has a value of 0.9 [64].

$$V_2 = V_1(1 - \frac{1-\sqrt{(1-C_T)}}{2}(1 + \frac{2.x}{\sqrt{1+4.x^2}})) \quad (4)$$

Where, V_1 is the WS before the first WT, x (m) is the distance between the first and second WTs, and V_2 is the WS before the second WT.

According to the work done in [62], the Cp is greatly affected by the value of both the TSR and the pitch angle (β). Therefore, to increase the value of this factor, the value of both β and the TSR must be changed, with the biggest value of Cp being when β takes the value 0°. To determine the value of Cp, equation (5) is used for this purpose.

In the WE generation system, the DFIG is used a lot for simplicity of control and ease of control compared to other generators [11, 15]. Also, the DFIG is distinguished by its robustness and low maintenance, as it is not exposed to many breakdowns, which makes it the most demanding for use in wind systems [16, 21]. As it is known, to produce current, we need ME to rotate the DFIG-DRWT. The Park transformation is employed to get the DFIG model [64]. Equation (6) represents the MM of the electric part of the DFIG, where the MM of the electric part is connected to voltage, current, and flux [62-67].

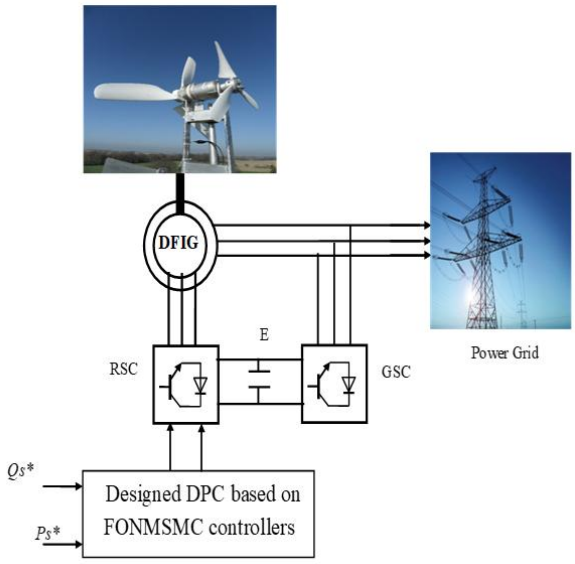

Fig. 2. Structure of the DFIG-DRWT.

$$C_p(\lambda,\beta)=\frac{1}{\lambda+0.08\beta}-\frac{0.035}{\beta^3+1} \tag{5}$$

$$\begin{cases} V_{ds}=R_sI_{ds}+\dfrac{d\phi_{ds}}{dt}-w_s\phi_{qs} \\ V_{dr}=R_rI_{dr}+\dfrac{d\phi_{dr}}{dt}-(w_s-w_r)\phi_{qr} \\ V_{qs}=R_sI_{qs}+\dfrac{d\phi_{qs}}{dt}+w_s\phi_{ds} \\ V_{qr}=R_rI_{qr}+\dfrac{d\phi_{qr}}{dt}+(w_s-w_r)\phi_{dr} \end{cases} \tag{6}$$

Where, V_{qs} and V_{ds} are the quadrature and direct stator voltages (V), R_s is the stator resistance (Ω), V_{dr} and V_{qr} are the direct and quadrature rotor voltages (V), I_{qs} and I_{ds} are the quadrature and direct stator currents (A), ω_r is the electrical pulsation of the rotor (RPM), and R_r is the rotor resistance (Ω).

$$\begin{cases} \phi_{ds}=L_sI_{ds}+MI_{dr} \\ \phi_{dr}=L_rI_{dr}+MI_{ds} \\ \phi_{qs}=L_sI_{qs}+MI_{qr} \\ \phi_{qr}=L_rI_{qr}+MI_{qs} \end{cases} \tag{7}$$

Where, ϕ_{ds} and ϕ_{qs} are the direct and quadrature stator fluxes (Wb), ϕ_{dr} and ϕ_{qr} are the direct and quadrature rotor fluxes (Wb), M is the mutual inductance (H), and L_r is the rotor inductance (Wb).

Equation (8) expresses the DFIG's mechanical component [61].

$$J\cdot\frac{d\Omega}{dt}+f\cdot\Omega=T_e-T_r \tag{8}$$

Where, T_e is the torque (N·m), f is the viscous friction coefficient (N·s/m^2), p is the number of pole pairs, J is the inertia (kg·m^2), Ω is the mechanical rotor speed (RPM), and T_r is the load torque (N·m).

The torque of the DFIG is represented in Equation (9) [64].

$$T_e=\frac{3}{2}p\frac{M}{L_r}(I_{dr}.\phi_{qs}-I_{qr}.\phi_{ds}) \tag{9}$$

The DFIG powers are related to voltage and current, where the value of both the *Ps* and *Qs* rises with the augment in voltage and current.

$$\begin{cases} Q_s=\dfrac{3}{2}(V_{qs}I_{ds}-V_{ds}I_{qs}) \\ P_s=\dfrac{3}{2}(V_{ds}I_{ds}+V_{qs}I_{qs}) \end{cases} \tag{10}$$

Typically, PI or hysteresis comparator regulators are employed to manage the power of DFIGs. While these controllers yield satisfactory results in terms of DR, they often fall short in delivering desirable PQ and current THD. Additionally, these controllers are less robust, particularly when there are changes to the system parameters.

Some solutions have been suggested in the literature to address the limitations of PI regulators. Among these solutions, nonlinear robust algorithms such as SMC and BC strategies have gained prominence. However, utilizing these nonlinear approaches typically requires a comprehensive understanding of the MM of the ES in question, which can make the control system vulnerable to variations in machine parameters.

To address these challenges, a new robust regulator is proposed that diverges from the existing controls in the literature. Importantly, this proposed robust regulator does not depend on an MM of the ES being studied. A detailed discussion of this new regulator will follow in the next section.

3. Proposed Robust FONMSMC Approaches

This section provides a detailed discussion of the new robust regulator for power control, focusing on its advantages and disadvantages. The approach designed in this paper relies on the fractional approach as an effective solution. As is well known, the fractional control approach is one of the most prominent strategies or solutions that have proven effective and efficient in the field of control.

In recent years, fractional calculus has emerged as an effective mathematical framework for modeling and controlling complex dynamical systems. Unlike traditional fractional calculus, fractional calculus allows for non-integer-order differentiation and integration, providing an additional degree of freedom that enhances system modeling accuracy and control performance. Fractional calculus-based controllers–commonly known as fractional controllers – offer greater flexibility in shaping system dynamics, improving robustness, and achieving superior transient and steady-state responses. Among these units, the fractional derivative integral proportional control (FOPID) has received considerable attention due to its ability to precisely adjust control parameters through fractional orders of integration and differentiation.

Fractional calculus has proven remarkably effective in various engineering fields, including electric motors, power systems, robotics, and renewable energy applications, where nonlinearity, parameter uncertainties, and external disturbances often weaken the performance of traditional control. By incorporating memory and genetic characteristics inherent in micro-actuators, these controllers can more accurately represent dynamic real-world behavior, leading to improved robustness, adaptability, and control accuracy. As a result, fractional calculus strategies have become an active research area, inspiring hybrid designs that combine micro calculus with modern smart technologies such as neural networks, FL method, and slip mode control, enhancing system flexibility and dynamic response.

The robust FONMSMC is presented as a promising solution in the field of energy, representing an improvement over the MSMC. To effectively address the modeling of the designer's approach, the MSMC will first be examined, with an emphasis on its limitations that hinder its broader application in control systems. In the following subsection, a detailed MM of the MSMC will be presented, along with its main advantages and disadvantages.

3.1 Design of the MSMC Technique

Traditionally, the SMC approaches were based on variable structure systems [68]. This technique is among the most widely used nonlinear approaches and the most popular among researchers because of its robustness compared to other controls [69]. This control can be accomplished easily, and it depends on the MM of the ES [70]. Equation (11), which represents the SMC technique, has two primary components: a continuous part and a discontinuous part [71].

$$w = w_n + w_{eq} \tag{11}$$

Where, w_{eq} and w_n are the continuous and discontinuous parts of the SMC technique.

The discontinuous control of the SMC is represented by Equation (12), where μ is the gain that modifies the usual SMC response [69].

$$w_n = \mu \times Sign(S) \tag{12}$$

Where, μ is the positive gain. S is the surface ($S = X^*-X$).

As for the continuous part, it is connected to the MM of the studied ES (parameters), as this part makes the SMC technique more complicated, especially in the case of complex ESs. Moreover, the biggest crisis of the SMC technique is the chattering crisis [72], which creates several drawbacks at the ES level, such as the WP generation ES. The use of the SMC to control an asynchronous generator creates oscillations in the torque, *Ps*, current, and *Qs* levels. Besides the chattering problem, the SMC in this way is complex and difficult to apply and execute in complex ESs. To simplify this controller, a novel design of the SMC is suggested to control the DFIG-DRWT system, and this is achieved by replacing the continuous part of the surface. This suggested method is called the MSMC. The first use of this control was to enhance the competence of the DPC [73]. Equation (13) represents the MSMC. The MSMC is simple, easy to realize in an embedded ES, and can be used in complex ESs. The suggested MSMC can be illustrated in Figure 3.

$$u(t) = \mu_1 \times Sign(S) + \mu_2 \times S \tag{13}$$

Where, μ_2 and μ_1 are the MSMC gains. S is the error (S=e).

The MSMC technique is not connected and linked to the studied ES or the ES parameters, as it is applied directly to the ES without resorting to complex calculations. To ensure the stability of this method, the Lyapunov's theory (LT) is used, where the Equations (14) and (15) are used to prove stability.

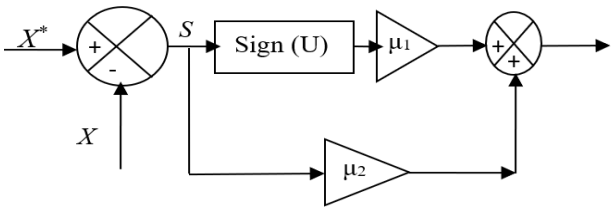

Fig. 3. MSMC approach.

$$S \times \dot{S} \prec 0 \tag{14}$$

$$V(x) = \frac{S^2}{2} \tag{15}$$

Where, $V(0) = 0$, $V(\infty) = \infty$.

To obtain information about the stability of the MSMC, the derivation Equation (15) is determinate. If $V(x) > 0$, $\dot{V}(x) < 0$, and $\forall x \neq 0$ then the ES is asymptotically stable.

Stability is achieved if Equation (16) is achieved.

$$\dot{V}(x) = \dot{S}(x) \times S(x) \prec 0 \tag{16}$$

The derivative V of must satisfy $\dot{V}(S) \leq -\eta|S|$ for finite-time convergence.

Where, η is the gain.

Substituting the control law:

$$\dot{S} = \dot{e}(t) = \dot{X}^* - X \tag{17}$$

For a stable system, $\dot{S}$ must be driven to zero. Using the control law:

$$\dot{S} = -\mu_1 \times Sign(S) - \mu_2 \times S \tag{18}$$

The requirement needs to be met to guarantee the finite time's convergence to the surface. According to the theory, the derivative must be negative to satisfy the stability condition. Also, to achieve the condition of stability, it must ensure convergence towards 0 at a certain time, so Equation (19) is used to achieve this condition.

$$\dot{V}(x) = \dot{S}(x) \times S(x) \prec -\eta|S| \tag{19}$$

Thus:

$$\dot{V}(S) = S.(-\mu_1 \times Sign(S) - \mu_2 \times S) = -\mu_2 S^2 \leq -\eta|S| \tag{20}$$

This ensures stability if $\mu_1 > \eta$ and $\mu_2 > 0$.

Based on research [73], the use of the MSMC does not eliminate power and current ripples. Additionally, in robustness testing, it is observed that this algorithm is slightly affected by the variable parameters of the studied system. Given these drawbacks, a new approach has been developed that utilizes NA algorithms and fractional calculus to enhance the robustness and efficiency of the MSMC. The following subsection details this new approach, highlighting its key advantages.

3.2 Design of the Proposed Robust Regulator

In this section, two distinct methods are essentially combined. Both fractional calculus and the feedforward backpropagation neural network (FBNN) are used to enhance the competence of the MSMC technique. FONMSMC is a hybrid nonlinear strategy that is simple and easy to realize.

The FBNN was adopted for its ease of use, high accuracy, and rapid DR. Furthermore, using the FBNN does not require precise data of the MM of the ES being studied, which enables it to produce satisfactory results even when machine

parameters change. Moreover, the fractional-order control strategy was adopted as a solution to enhance the performance of the MSMC due to its high strength, ease of use, and the lack of need to precisely know the MM of the ES under study. To implement the FONMSMC regulator, the FBNN is first applied to the MSMC regulator. After obtaining the FBNN method, the fractional-order control is applied to the NMSMC. Figure 4 represents the flowchart of the robust FONMSMC. This diagram represents the main steps in completing the designed controller.

The robust FONMSMC is illustrated in Figure 5. Therefore, the robust FONMSMC is a development of the MSMC. Also, the robust FONMSMC is not linked to the MM of the studied ES, as it can be applied directly to any ES, regardless of the level of complexity. From Figure 5, it can be seen that this robust method has small gains, which makes it easy to adjust. Also, the use of NA techniques increases the accuracy of the MSMC, increases the efficiency, and reduces energy consumption.

Among the most prominent advantages of robust FONMSMC can be mentioned:

- Reduced Chattering: Feedforward Backpropagation Neural Network smoothens the control signal.
- Fractional-order precision: Better handling of nonlinearities and disturbances.
- Adaptive Gains: FBNN adjusts gains dynamically for varying conditions.

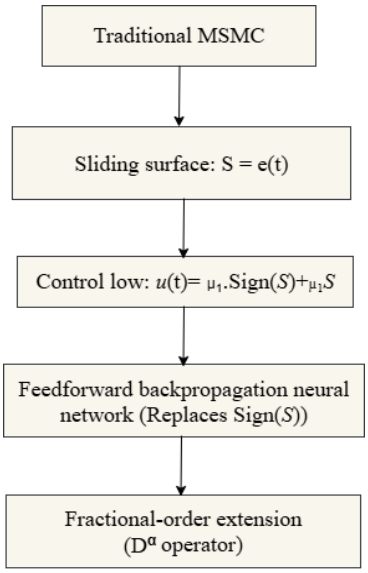

Fig. 4. Flowchart of the designed controller.

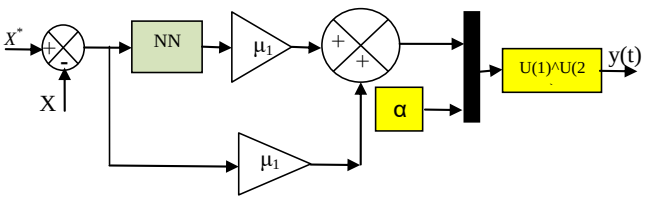

Fig. 5. Proposed robust FONMSMC technique.

This derivation ensures the robust FONMSMC method is adaptive, robust, and suitable for complex systems like DRWT turbines.

In this work, a FBNN was used to implement the robust controller. Newff is used in MATLAB to implement the FBNN technique. As is well known, FBNN techniques are based on learning. The Conjugate gradient with Beale-Powell restarts algorithm (CGBPRA) was used to realize the FBNN technique. The CGBPRA is the most efficient and effective FBNN in terms of training accuracy. This algorithm is one of the conjugate gradient methods used in unconstrained optimization. It combines nested updates and a great conjugate to help improve the conjugateness, especially for no quadratic functions. This method is particularly useful for large-scale optimization problems because it does not require storing matrices. The implementation of the CGBPRA relies on knowledge of the output and input data of the regulator to be reconfigured by the FBNN technique.

In MATLAB, traincgb is used to execute the CGBPRA. The basic idea of this algorithm is based on testing the orthogonality between successive gradients.

In this work, a FBNN based on CGBPRA technique is proposed to compensate the Sign(U) function of MSMC controller for DFIG powers (*Ps* and *Qs*).

To embody the new regulator, the suggested model, referred to as the robust FONMSMC technique, is trained using the CGBPRA, typically optimizing the parameters of a FBNN or a similar model to minimize the performance function, typically the sum of squared errors. This training is performed using the MSMC. The training process is carried out according to the following steps:

Model definition and initialization:

- The MSMC model is defined, potentially incorporating NN architecture.
- Initial weights and biases of the FBNN or parameters of the MSMC model are randomly or heuristically initialized.

Data preparation:

- A dataset is prepared, consisting of input-output pairs. This data is typically split into training, validation, and testing sets.

Performance function definition:

- A performance function, commonly the sum of squared errors or mean squared error, is defined to quantify the discrepancy between the model's output and the actual target values.

Iterative optimization with Conjugate gradient with Beale-Powell restarts algorithm:

- Line Search: Determine a step size αk along the direction dk that minimizes f(xk+αkdk). Common line search methods include Wolfe conditions or the Armijo rule.
- Update Position: xk+1=xk+ αkdk.

- Compute New Gradient: gk+1=∇ f(xk+1)
- Beale-Powell Restart Check:

  If $|g_{k+1}^{T} g_k| \geq c\|g_k\|^2$ (where *c* is a chosen constant), then rest the search direction: $d_{k+1} = -g_{k+1}$

  Otherwise (if the restart condition is not met), compute the new search direction using a chosen Conjugate Gradient formula (e.g., Polak-Ribière, Fletcher-Reeves, Hestenes-Stiefel). For example, using Polak-Ribière:

$$d_{k+1} = -g_{k+1} + \beta_k d_k \quad (21)$$

  where $\beta_k = \frac{g_{k+1}^{T}(g_{k+1}-g_k)}{\|g_k\|^2}$

- Increment: k=k+1.

Convergence criteria:

- The training process continues iteratively until a predefined convergence criterion is met. This could be a maximum number of epochs, a minimum error threshold on the validation set, or a sufficiently small change in the parameters.

Validation and testing:

- During training, the model's performance is periodically estimated on the validation set to prevent overfitting.
- After training, the final performance of the trained MSMC model is assessed on the unseen test set.

To implement the algorithm, it is essential to first define several key parameters: the number of outputs, the acceptable error value, and the number of inputs, the number of cells in each layer, and the number of internal layers. Table 1 outlines the characteristics of the CGBPRA used for training the neural controller responsible for managing both *Ps* and *Qs*.

Derivation Steps:

Fractional-order extension:

Applying fractional control to the NMSMC regulator output using a fractional-order operator of type D^{α}.

The control law becomes:

$$y(t) = D^{\alpha}(\mu_1 \times (Neural) \times S + \mu_2 \times S \quad (22)$$

Where αrepresents fractional-order controls and S is the error or surface. μ_1 and μ_2 are the controller gains. These gains are used to adjust and change the DR, and these two values must be different from the value 0.

Neural network integration:

A neural network replaces the discontinuous sign(U) function to reduce chattering. The NN output is trained to approximate the optimal control action:

$$eural(S) = NN(S, \theta) \quad (23)$$

Where θ represents the NN weights.

Table 1. Features of NA technique used.

Parameters	Values
Number of neurons in layer 1	2
Train Param.goal	0
Functions of activation	Tansig, purelin, and traincgb
Train Param.eposh	200
Performances	Mean Squared Error (mse)
Number of neurons in hidden layer	50
Training	CGBPRA
Coeff of acceleration of convergence(mc)	0.9
Train Param.mu	0.8
Number of neurons in layer 2	1
Train Param.Lr	0.05
Train Param.show	50

Final FONMSMC control law:

$$y(t) = (\mu_1 \times (Neural) \times S + \mu_2 \times S)^{\alpha} \quad (24)$$

The NN is trained offline using data from the system dynamics. Compared to the MSMC regulator, the new regulator is more complex, making it more expensive. Also, the designed approach offers a number of advantages over the MSMC.

Depending on the value of α, the type of robust FONMSMC can be selected. If α takes the value of 1, the robust FONMSMC becomes an NMSMC. For the FONMSMC to be valid, α must not take the value 0. If α does not take the value 1 or 0, the controller becomes the FONMSMC. Therefore, this feature does not exist in other approaches, which makes the robust FONMSMC of major importance in the field of control, as it plays the role of two different approaches at the same time, and it is possible to pass from one control to another by setting α to 1.

Figure 6 represents the organization of the FBNN method applied in this study to embody the sign(U) function of the MSMC. This FBNN method consists of two layers: layer 2 and layer 1.

Figure 7 represents the structure of the two layers that make up the FBNN method. The gain values of the robust FONMSMC can be estimated using advanced algorithms like GA and PSO. However, implementing these algorithms often involves writing complex programs, and the results can be unsatisfactory, necessitating multiple repetitions of the process, which is not ideal.

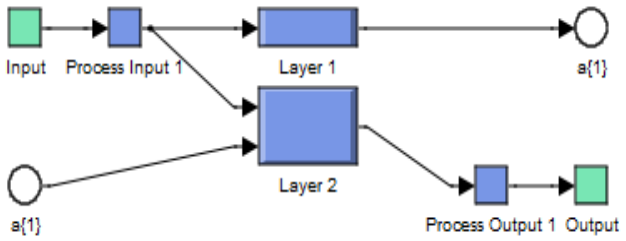

Fig. 6. FBNN controller.

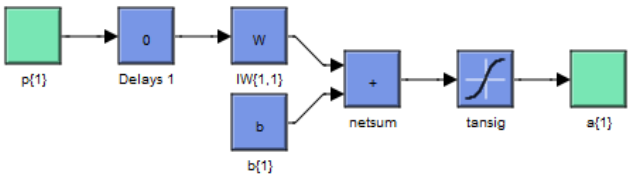

a) Layer 1

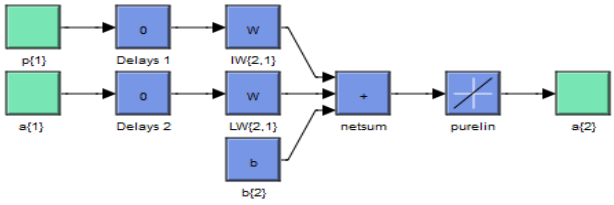

b) Layer 2

Fig. 7. Structure interne of the FBNN technique.

Therefore, a simpler, more efficient method has been employed to estimate the gain values for the robust FONMSMC. This control focuses on simulation and experimentation, avoiding the need for intricate programming while still yielding excellent results. The values selected during this process have demonstrated significant improvements in power and current fineness. In the following section, the application of the robust FONMSMC will be explored to address the shortcomings of the DPC. All relevant details regarding the designed DPC will be provided, including its advantages and disadvantages.

4. Proposed Robust Control Approach

Traditionally, the DPC approach of the DFIG is among the most popular approaches with the DTC approach because of its ease, robustness, and ease of use to control EMs [74]. This technique relies on the use of an ST and two electrical power HCs. The DPC technique has several benefits, but it also has some drawbacks, including current, and *Ps* and *Qs* destructive ripples [75]. Also, the frequency is not fixed due to the use of HCs. Moreover, this control provides a greater value for the current THD [76, 73].

In this section, a new idea is presented to adjust the DFIG-DRWT energy. The DPC based on robust FONMSMC (DPC-FONMSMC) is an amendment of the DPC, where both the robust FONMSMC and PWM technique are used to enhance the superiority of the *Qs*/*Ps* and the current. Also, to minimize the fluctuations of torque, flux, *Qs*/*Ps*, and current. Figure 8 represents the nonlinear DPC-FONMSMC for regulating the DFIG-based variable-speed DRWT systems.

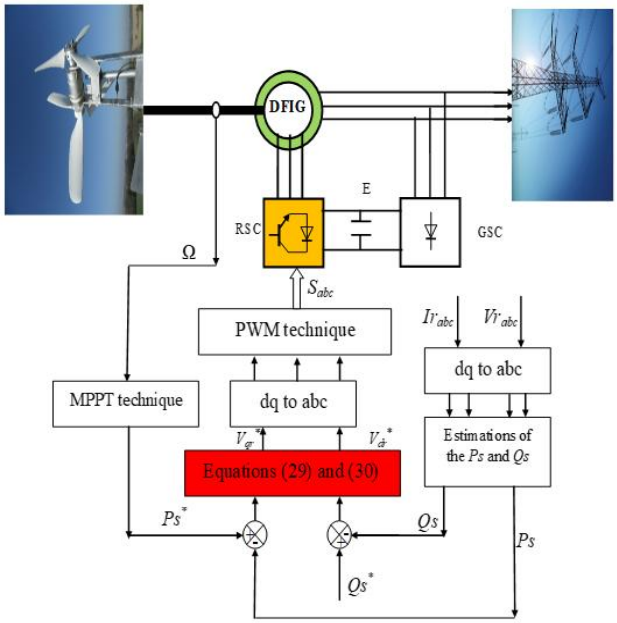

Fig. 8. Robust DPC-FONMSMC approach of the DFIG-DWRT.

The robust FONMSMC is used to estimate VRVs based on energy errors. Therefore, this new algorithm uses power estimation to calculate power errors. The energy estimation used in this new algorithm is the same as that used in the DPC. In this studied ES, the MPPT is employed and used to get the *Ps* reference (Ps^*), and on the other hand, the *Qs* reference (Qs^*) is set at the value 0 VAR. The robust DPC-FONMSMC technique is an adjustment and intelligent amelioration of the DPC, where the PWM is employed and used instead of the ST, and the designed FONMSMC is used instead of the HCs.

The robust DPC-FONMSMC is easy and uncomplicated. Also, the robust DPC-FONMSMC is solid and is not affected by the modification in the parameters of the DFIG or the studied ES compared to the DPC. The robust DPC-FONMSMC minimizes the fluctuations of torque, current, *Qs*/*Ps*, and flux compared to other techniques.

In the robust DPC-FONMSMC, both the estimation of *Qs* and generated *Ps* are utilized, similar to the DPC. This process requires the measurement of both voltage and supplied ES current, as well as an understanding of the flux in both the rotor and stator of the DFIG-DRWT.

To calculate the stator flux (ϕ_s) and the rotor flux (ϕ_r), Equation (25) is used.

$$\begin{cases} \phi_{s\alpha} = \int_0^t (V_{s\alpha} - R_s I_{s\alpha}) dt \\ \phi_{s\beta} = \int_0^t (V_{s\beta} - R_s I_{s\beta}) dt \\ \phi_{r\alpha} = \int_0^t (V_{r\alpha} - R_r I_{r\alpha}) dt \\ \phi_{r\beta} = \int_0^t (V_{r\beta} - R_r I_{r\beta}) dt \end{cases} \quad (25)$$

The amplitudes of both stator and rotor flux (ϕ_r and ϕ_s) are given by Equation (26).

$$\begin{cases} \phi_s = \sqrt{\phi_{s\alpha}^2 + \phi_{s\beta}^2} \\ \phi_r = \sqrt{\phi_{r\alpha}^2 + \phi_{r\beta}^2} \end{cases} \quad (26)$$

Equation (27) represents the stator/rotor flux angles.

$$\begin{cases} \theta_s = arctg(\dfrac{\phi_{s\beta}}{\phi_{s\alpha}}) \\ \theta_r = arctg(\dfrac{\phi_{r\beta}}{\phi_{r\alpha}}) \end{cases} \quad (27)$$

The *Ps* and *Qs* are estimated using the formulas from Equations (25) and (26). The estimation of the DFIG-DRWT power is represented by Equation (28) [75, 73].

$$\begin{cases} Q_s = -\dfrac{3}{2}(\dfrac{Vs}{\sigma.Ls} \cdot \phi_{r\beta} - \dfrac{Vs.Lm}{\sigma.Ls.Lr} \cdot \phi_{r\alpha}) \\ P_s = -\dfrac{3}{2}\dfrac{Lm}{\sigma.Ls.Lr} \cdot (Vs.\phi_{r\beta}) \end{cases} \quad (28)$$

Equation (29) represents the stator flux in the two axes (α and β).

$$\begin{cases} \phi_{s\alpha} = L_r I_{r\alpha}(1 - \dfrac{M^2}{L_r L_s}) + \dfrac{M}{L_s}\phi_s \\ \phi_{s\beta} = \sigma L_r I_{r\beta} \end{cases} \quad (29)$$

The relationship between flux, stator voltage and electrical impulse can be represented by Equation (30).

$$|\overline{\phi_s}| = \frac{|\overline{V_s}|}{w_s} \quad (30)$$

According to the works [74, 76] the powers can be written by Equation (31).

$$\begin{cases} P_s = -\dfrac{3}{2}\dfrac{Lm}{\sigma.Ls.Lr} w_s |\phi_s||\phi_r| \sin(\lambda) \\ Q_s = -\dfrac{3}{2}\dfrac{ws}{\sigma.Ls}|\phi_s|(\dfrac{M}{Lr}|\phi_r|\cos(\lambda) - |\phi_s|) \end{cases} \quad (31)$$

Equation (32) expresses the derivative of both *Qs* and *Ps*.

$$\begin{cases} \dfrac{dP_s}{dt} = -\dfrac{3}{2}\dfrac{Lm}{\sigma.Ls.Lr} w_s |\phi_s| \dfrac{d(|\phi_r|\sin(\lambda))}{dt} \\ \dfrac{dQ_s}{dt} = -\dfrac{3}{2}\dfrac{M.ws}{\sigma.L_r Ls}|\phi_s|(\dfrac{d(|\phi_r|\cos(\lambda))}{dt}) \end{cases} \quad (32)$$

In the robust DPC-FONMSMC, a control concept for both *Ps* and *Qs* is established. The robust FONMSMC has been designed to regulate the energy of the DFIG-DRWT. This regulator operates with a single input and a single output: the input represents the power error (e_r and e_a), while the output generates the reference rotor voltages (V_{dr}^* and V_{qr}^*).

Equations (33) and (34) define the robust FONMSMC for *Qs* and *Ps*, respectively. Notable advantages of this control include its simplicity, robustness, and ease of implementation.

$$V_{qr}^* = (\mu_1 \times (neural) \times e_a + \mu_2 \times e_a)^{\alpha} \quad (33)$$

$$V_{dr}^* = (\mu_1 \times (neural) \times e_r + \mu_2 \times e_r)^{\alpha} \quad (34)$$

Where, e_r is the error of the *Qs* ($e_r = Q_s^* - Q_s$).μ_1 and μ_2 are the gains. e_a is the error of the *Ps* ($e_a = P_s^* - P_s$).

Figure 9 represents the CGBPRA training for the robust FONMSMC for the *Ps* and *Qs*, where the features of FBNNs are used to ameliorate the characteristics of the MSMC for the *Qs*/*Ps*, and they are represented in Figures 10 and 11.

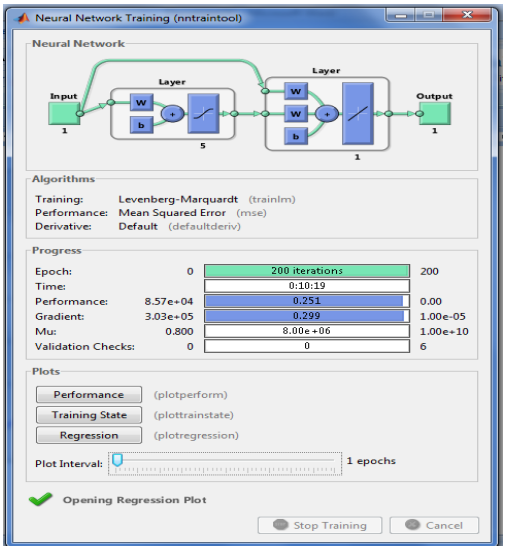

Fig. 9. CGBPRA training.

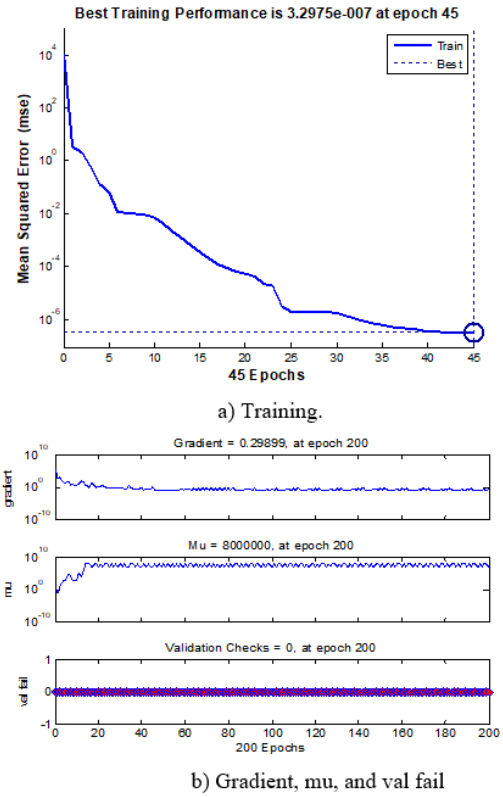

a) Training.

b) Gradient, mu, and val fail

Fig. 10. Characteristic of the CGBPRA for FONMSMC. controller of *Ps*.

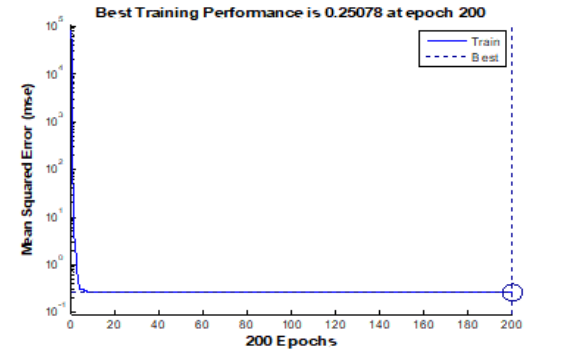

a) Training.

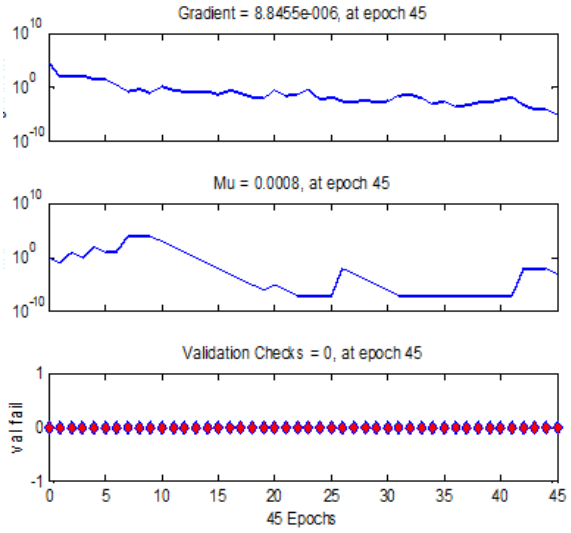

b) Gradient, mu, and val fail

Fig. 11. Characteristic of the CGBPRA for robust FONMSMC of Qs.

Figure 12 represents the schematic diagram of the algorithm designed in this study to control the powers of the DFIG. Figure 12a represents the robust FONMSMC of Ps. In addition, the robust FONMSMC method of Qs is represented in Figure 12b. This control is simple and more durable compared to other approaches, such as the PI regulator. This algorithm was used to reduce the Ps and Qs ripples and ameliorate the quality and minimize the THD of the generated ES current of the DFIG-DRWT.

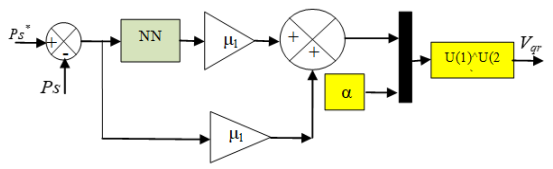

a) *Ps*.

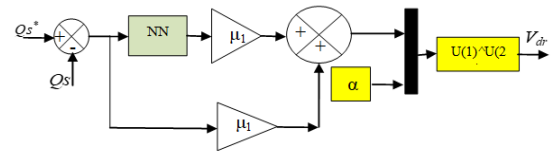

b) *Qs*.

Fig. 12. Proposed robust power controller.

To demonstrate the stability of the new algorithm, we can use either the LT or the Bode curve method. The LT method is well-known as a mathematical technique that involves derivations to determine stability conditions. However, this method can sometimes involve complex calculations. In contrast, the Bode curve is simple, graphical, and user-friendly, requiring no complicated computation. This method utilizes MATLAB to generate phase and magnitude plots. Stability is established through the assessment of both the phase margin and gain margin.

For this paper, the Bode curve has been selected to validate the stability of the new algorithm. Figure 13 illustrates the Bode curve for the two control methods. In Figure 13a, it is evident that both the Magnitude and Phase change with frequency, attaining negative values. The Magnitude ranges from -48 dB to -250 dB, while the Phase ranges from 0 to -270 degrees. Notably, when the Phase reaches -180 degrees, the Magnitude is approximately -70 dB, indicating a gain margin of 70 dB. Since this gain margin is positive, we conclude that the MSMC is stable. Figure 13b displays the Bode curve for the robust FONMSMC. Here, the Phase varies from 0 to -270 degrees, and the Magnitude ranges from -48 dB to 200 dB. When the Phase is -180 degrees, the Magnitude is approximately -60 dB. Therefore, the value of the gain margin is approximately equal to 60 dB. Since the value of the gain margin is positive, the robust FONMSMC is stable.

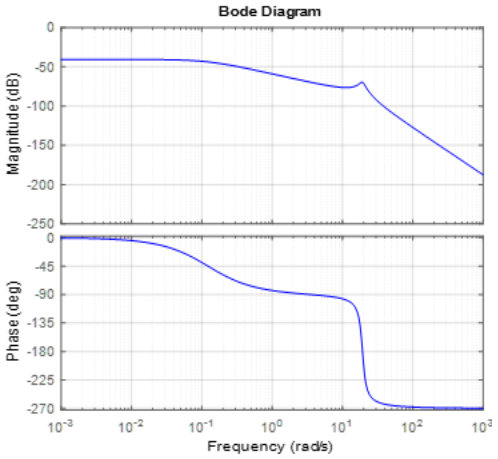

a) DPC-MSMC

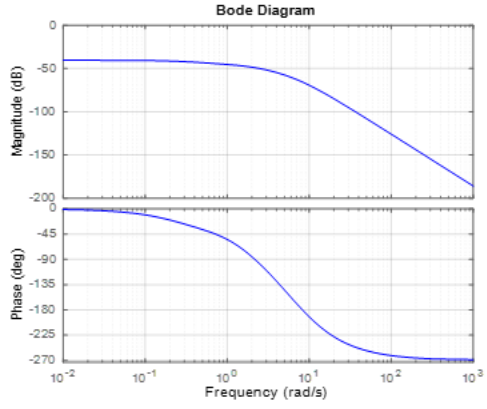

b) Robust DPC-FO-NMSMC

Fig. 13. Bode curve of both techniques.

5. Results

In this section, the validity, competence, efficacy, and performance of the robust FONMSMC for DFIG-DRWT are demonstrated using MATLAB 2014. The competence is compared with the MSMC. The comparison between the two algorithms is made in terms of reference tracking, robustness, PQ, RT, etc.

Two different WS profiles are used to study the efficacy of the new algorithm. This new algorithm is applied on the machine's inverter only, where a 1.5 MW generator is used. The parameters of the used WTs are as follows: R_2=25.5 m, r_1=1 m, J_1=500 kg.m^2, r_2=0.5 m, R_1=13.2 m, r_g=0.75 m, J_2=1000 kg.m^2.

The DFIG parameters are: p = 2, L_r = 0.0136 H, 380/696 V, R_s = 12 mΩ, L_s = 13.7 mH, 50 Hz, J = 1000 kg.m^2, L_m = 13.5 mH, R_r = 0.021 Ω, and f_r = 0.0024 N·m/s [61, 63].

5.1 Test 1: Variable WS Profile

In this study, we examine the efficiency of the robust FONMSMC under varying WS. The results obtained are compared with those from the MSMC.

Figure 14 illustrates the WSs used in this test, while the graphical and numerical results are shown in Figure 15 and in Table 2.

Figure 15a illustrates the variation in *Qs* over time for the two techniques. This energy closely follows the reference, displaying some ripples. Notably, these fluctuations are more pronounced when using the MSMC compared to the proposed robust FONMSMC. Both strategies exhibit a rapid DR. The value of this power remains constant at 0 VAR, regardless of variations in WS. The reference value for *Qs* was set to 0 VAR to achieve a power factor of 1.

Figure 15b shows the variation in *Ps* over time for both control strategies. This power also closely aligns with the reference for both controllers, demonstrating a fast DR. The fluctuations in this energy correspond to changes in WS, resulting in some negative values. It is evident from this figure that the energy fluctuations are significantly reduced when using the robust FONMSMC compared to the MSMC. Figure 15c depicts the torque variations for the two regulators. The torque for both controllers reflect variations in active power, exhibiting a rapid DR. However, ripples can be observed in the torque values. Additionally, the torque has a negative value, indicating that the DFIG is generating energy and supplying it to the grid.

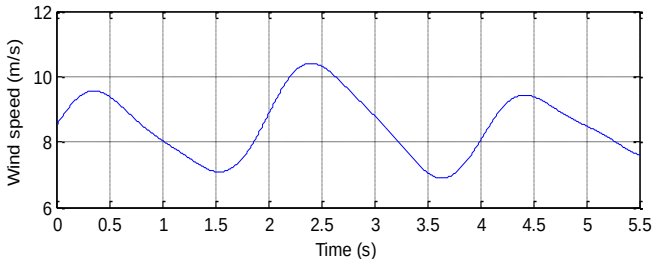

Fig. 14. Variable WS profile.

Figure 15d illustrates the variation in current over time for the two strategies. Both techniques exhibit a sinusoidal current shape, with the proposed technique demonstrating a significant quality advantage over the MSMC. Additionally, the current values for both strategies vary depending on changes in WS. As WS increases, the current value rises, and conversely, it decreases when WS decreases.

Figures 15e and 15f present the amplitude of the fundamental signal (FS) and the THD values for both control methods. According to these figures, the THD value is 0.48% for the robust DPC-FONMSMC and 0.84% for the MSMC. This indicates that the new algorithm significantly minimizes the THD compared to the MSMC, with a reduction of 42.86%. This demonstrates that the robust FONMSMC is highly effective in ameliorating current fineness compared to the MSMC. Also, the amplitude of the FS at 50 Hz is 843 A for the MSMC and 842.80 A for the robust FONMSMC.

Thus, the amplitude value is slightly better with the MSMC. Therefore, the amplitude performance of the robust FONMSMC may be considered a drawback in this instance. This disadvantage may stem from the gain values of the robust FONMSMC, which could be addressed in future improvements by incorporating additional methods.

Figure 16 provides a close-up view of the results from test 1. It shows that the undulations in torque, energy, and current are lower in the robust FONMSMC compared to the MSMC. In the MSMC, the estimated ripples for torque, *Ps*, current, and *Qs* were 53.34 N·m, 12000 W, 16 A, and 12664 VAR, respectively.

In contrast, the FONMSMC demonstrated significantly lower undulations, with values of 8 N·m, 2000 W, 2.40 A, and 2479.04 VAR for torque, power, current, and *Qs*, respectively. As a result, the robust FONMSMC achieved reductions in the ripples of torque, power, current, and Qs by 85%, 83.33%, 85%, and 80.42%, respectively.

The ripple reduction ratios obtained in this power test are illustrated in Figure 17. These ratios highlight the efficiency of the algorithm in enhancing the fineness of current and energy, making it a promising solution for applications in other fields.

Table 2 presents the numerical results from test 1, where both controls were utilized. The table includes the values and minimization ratios for the RT, SSE, and overshoot. The results show that the robust FONMSMC significantly diminutive the SSE of DFIG energy when compared to the MSMC, with reduction ratios of 89.08% for Ps and 62.04% for Qs, respectively. However, regarding the overshoot of Qs, the robust FONMSMC performed unsatisfactorily compared to the MSMC, which achieved an estimated reduction of 80.07% in overshoot.

In contrast, for the overshoot of Ps, the robust FONMSMC yielded satisfactory results, with a reduction percentage of 50.68%. These reduction ratios are visually represented in Figure 18.

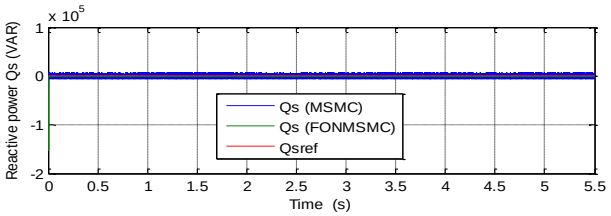

a) Reactive power.

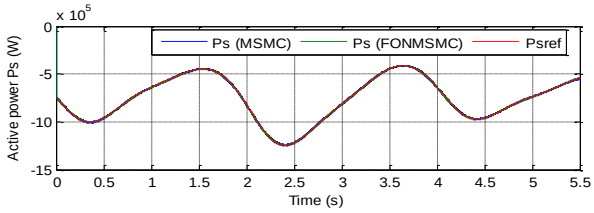

b) Active power.

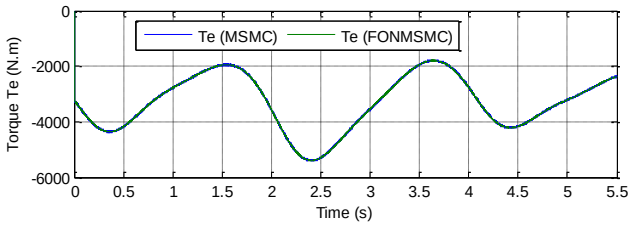

c) Torque.

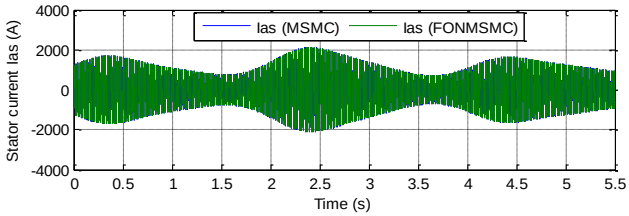

d) Current I_{as}.

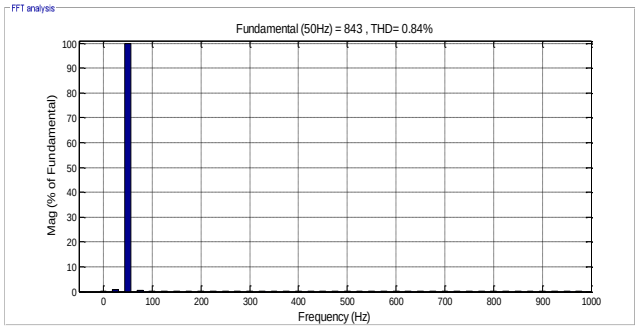

e) THD (MSMC).

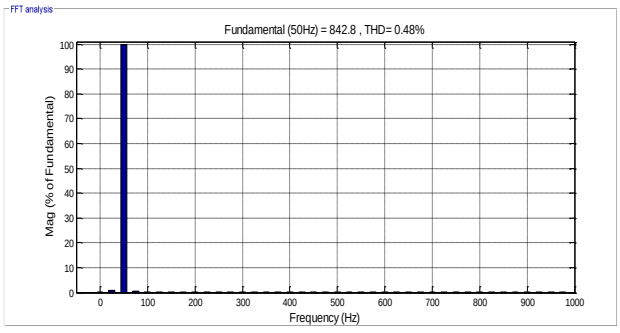

f) THD (FONMSMC).

Fig. 15. First test results.

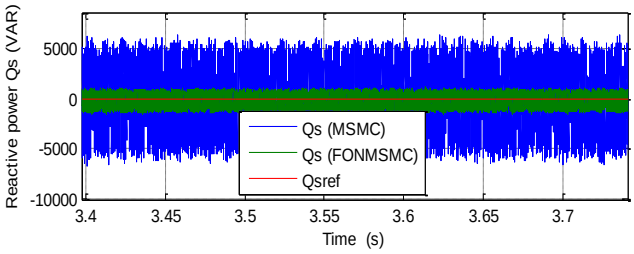

a) Reactive power.

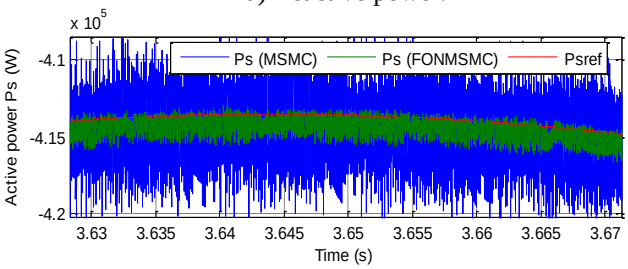

b) Active power.

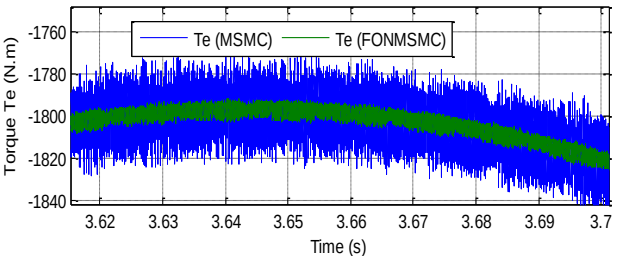

c) Torque.

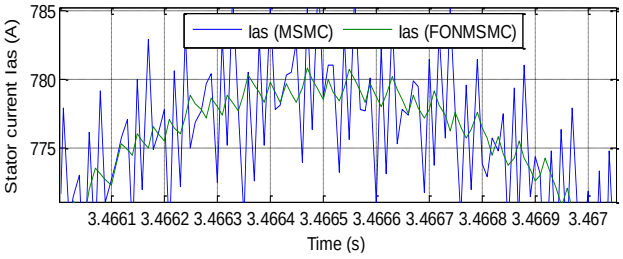

d) Current I_{as}.

Fig. 16. Zoom in the first test results.

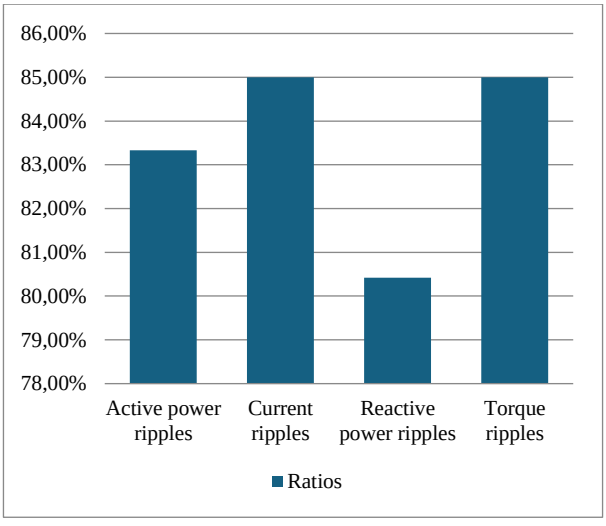

Fig. 17. Ripple reduction ratios in the test 1.

Table 2. Reduction rates in the test 1 case.

Techniques and ratios		*Ps* (W)	*Qs* (VAR)
MSMC	Overshoot	2190	2426.18
	SSE	2080	1370.75
	RT (ms)	1.14	1.14
FONMSMC	Overshoot	1080	483.43
	SSE	40	520.40
	RT (ms)	4.32	4.32
Ratios (%)	Overshoot	50.68	80.07
	SSE	89.08	62.04
	RT (ms)	-73.61	-73.61

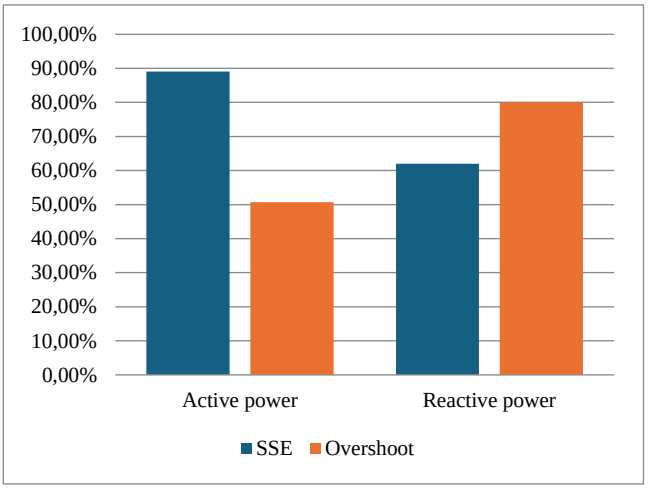

Fig. 18. Minimization ratios for overshoot and SSE.

The MSMC also demonstrated significantly better power RT than the robust FONMSMC, with power RT minimized by an estimated rate of 73.61% for both *Ps* and *Qs*. Therefore, the algorithm proposed in this test can be considered effective for addressing negative power RT. This negativity may be linked to the gain values of the new robust algorithm and the features of the FBNN approach used. Possible future improvements could involve employing different strategies, such as the PSO algorithm. Additional research will explore effective solutions to tackle this issue.

5.2 Test 2

In this test, we evaluate the efficacy and performance of the robust FONMSMC using a different WS profile than that used in the first test. Figure 19 displays the WS profile employed in this assessment to compare the efficiency and effectiveness of the robust FONMSMC against the MSMC. The results are illustrated in Figures 20 and 21, and Table 3 summarizes the findings from this test.

Figure 20a illustrates the change in *Qs* over time for the two control strategies. The graph shows that *Qs* remains constant at the value of 0 VAR and does not vary with variations in WS. Additionally, there are fluctuations present in this power measurement, but these undulations are significantly diminished when using the robust FONMSMC compared to the MSMC.

Figure 20b depicts the variation in *Ps* over time for both control methods. It is important to note that negative values for *Ps* indicate that the system is generating power. The *Ps* exhibit a rapid DR for both controls, accompanied by ripples. However, these ripples are less pronounced when utilizing the robust FONMSMC in contrast to the MSMC. The *Ps* value varies according to changes in WS, decreasing as WS drops and increasing as WS rises.

Figure 20c portrays the torque variation for the two regulators. Similar to the previous measurements, this torque shows a rapid DR with fluctuations. The torque values can also become negative because the DFIG is generating power. Furthermore, the torque variation for both regulators mirror the variation in WS due to the implementation of the MPPT.

Figure 20c illustrates the torque variation for the two algorithms. This torque exhibits a rapid DR accompanied by ripples. Additionally, the torque can take on negative values because the DFIG is generating power. Notably, the torque variation for both controllers follow a similar pattern to the WS variation, which is a result of employing the MPPT.

Figure 20d depicts the current variation over time for the two control techniques. It can be observed that the current varies according to the changes in the shape of the WS. Furthermore, the current for both control strategies assume a sinusoidal form. The ripples in current are diminutive when using the robust FONMSMC, compared to the MSMC, aligning with the results from the first test. These findings underscore the efficiency and high performance of the robust FONMSMC, highlighting its potential for future interest.

Figures 20e and 20f show the THD values for the two methods. It is noted that the THD values were 0.30% for MSMC and 0.18% for robust FONMSMC. This indicates that the robust FONMSMC significantly diminishes the THD compared to MSMC, achieving a minimization of approximately 40%. This minimization signifies a higher quality of current with the robust FONMSMC compared to the MSMC. Moreover, the amplitude value of the FS (50 Hz) for the current was consistent at 2386 A for both techniques, demonstrating their equivalent performance in this test.

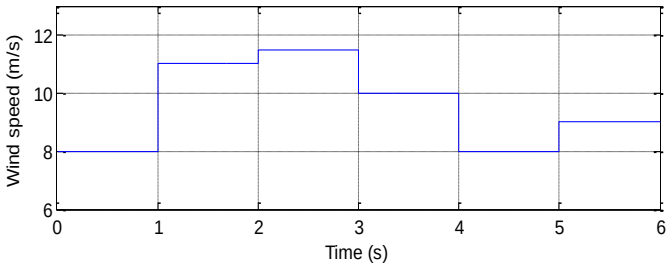

Fig. 19. Steps WS profile.

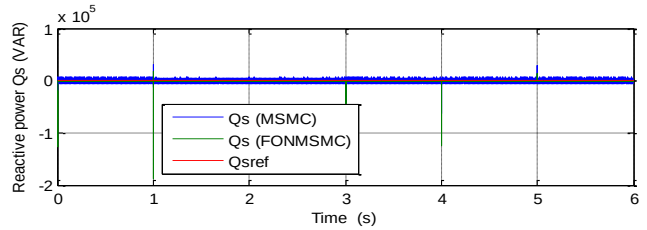

a) *Qs*.

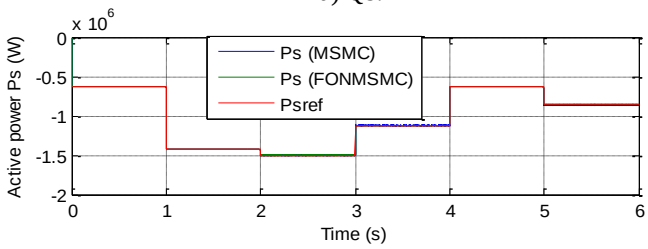

b) *Ps*.

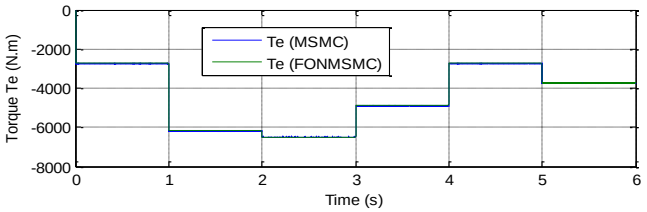

c) Torque.

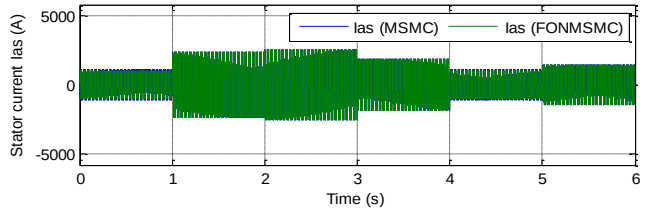

d) Stator current I_{as}.

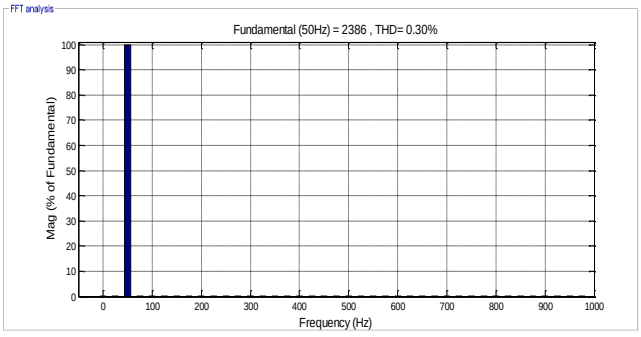

e) THD (MSMC)

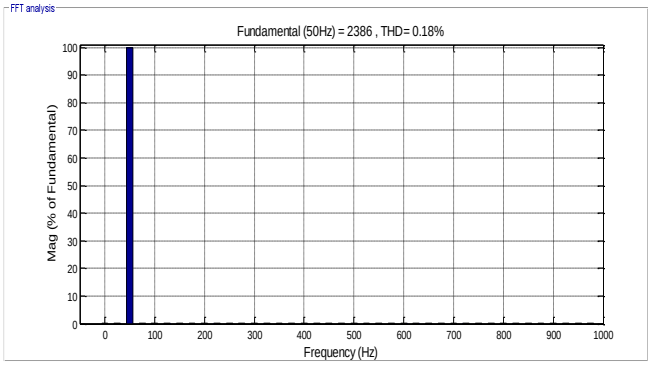

f) THD (FONMSMC).

Fig. 20. Test 2 results.

Figure 21 shows a zoomed-in view of the results of the second test. From this figure, the fluctuations for current, energy, and torque are significantly lower in the new robust algorithm compared to the MSMC. The ripples for the MSMC were estimated to be 16 A, 12673.40 VAR, 50 N·m, and 11150 W for current, *Qs*, torque, and *Ps*, respectively. In the new robust algorithm, these ripple values were 3.24 A, 2500 VAR, 10 N·m, and 2000 W for current, *Qs*, torque, and *Ps*, respectively.

From these values, the new robust algorithm diminishes the ripple values for current, *Qs*, torque, and *Ps* by 79.75%, 80.27%, 80%, and 82.06%, respectively. These obtained ratios are listed in Figure 22. Therefore, it can be said that the new robust algorithm is highly effective in enhancing the fineness of current and power, making it a highly valuable solution in the industrial field.

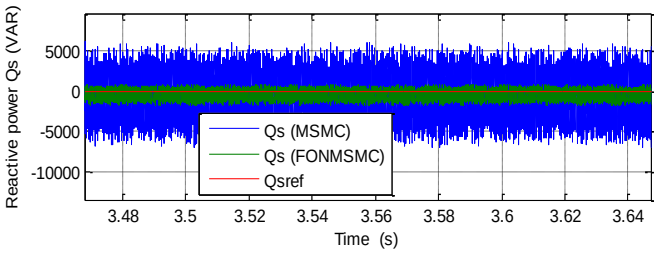

a) *Qs*.

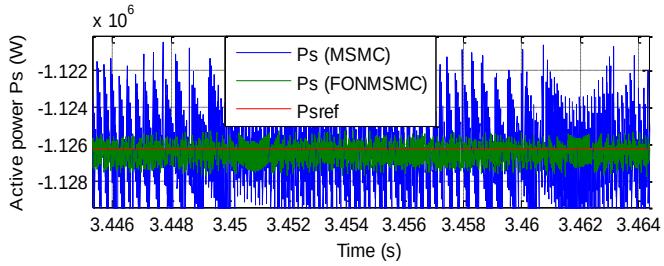

b) *Ps*.

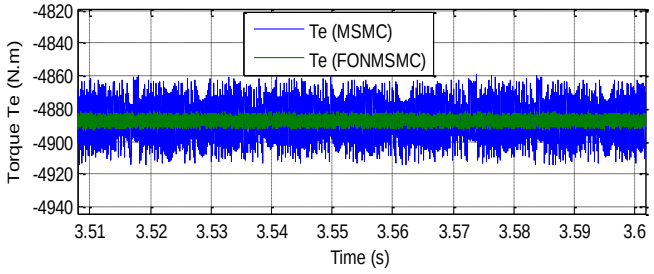

c) Torque.

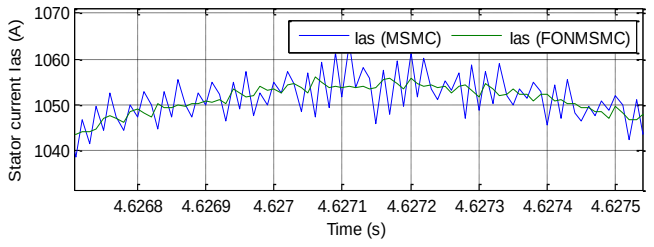

d) Stator current I_{as}.

Fig. 21. Zoom in the second test results.

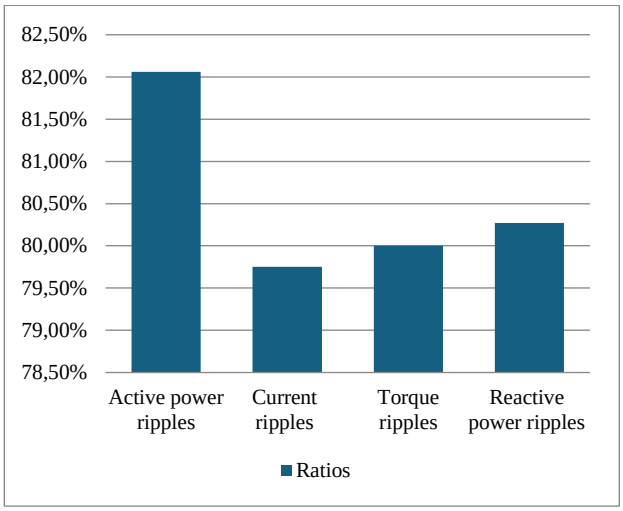

Fig. 22. Ripple reduction ratios in the second test.

In Table 3, the values and reduction ratios for fluctuations, SSE, RT, and overshoot related to DFIG energy are presented. It is observed that the robust FONMSMC significantly minimized the values of SSE and overshoot for *Ps* when compared to the MSMC, with reductions estimated at 92.47% and 53.07%, respectively. For *Qs*, the minimization percentage for SSE was 89.15%. According to the table, the MSMC yielded unsatisfactory results concerning the power RT and *Qs* overshoot. However, the MSMC did reduce the RT values by 72.57% for Ps and 73.09% for *Qs*. Consequently, the RT of the powers can be regarded as a downside of the new robust algorithm.

Furthermore, the new algorithm showed unsatisfactory performance in this test with regard to the overshoot value when compared to the MSMC. The reduction ratios from this test are illustrated graphically in Figure 23. These shortcomings can be attributed to the gain values used in the new robust algorithm. Future enhancements could address these issues by incorporating modifications to the designed new robust algorithm, such as employing a neural-modified SVM or a GA technique to compute the gain values more effectively.

Table 3. Reduction rates in the second test case.

Techniques and ratios		***Ps* (W)**	***Qs* (VAR)**
MSMC	Overshoot	2280	98.31
	SSE	2920	1000
	RT (ms)	0.96	0.95
FONMSMC	Overshoot	1070	800
	SSE	220	108.50
	RT(ms)	3.50	3.53
Ratios (%)	Overshoot	53.07	-87.71
	SSE	92.47	89.15
	RT (ms)	-72.57	-73.09

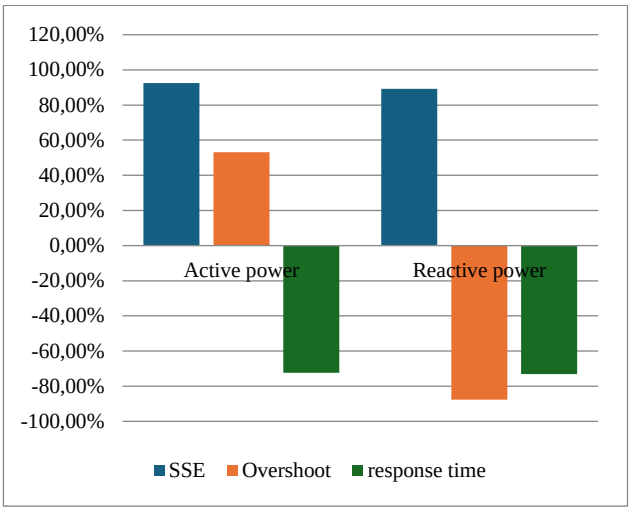

Fig. 23. Graphical representation of the reduction ratios for the second test.

Table 4 presents a study on the variations in both the amplitude of the FS (50 Hz) and the THD of current when using two different algorithms. The results from the first and second tests are included in this analysis. From the table, it is evident that both THD and amplitude values are significantly influenced by altering the waveform shape when both controls are implemented. Specifically, the THD value in test 2 shows a notable decrease compared to test 1 for both control methods. The difference in THD values between the two tests was measured at -0.30% for the new robust algorithm and -0.54% for the MSMC. The new robust algorithm achieved a THD reduction of approximately 62.50% in test 2 compared to the first. In comparison, the MSMC resulted in a 64.29% reduction. Thus, the new robust algorithm demonstrated a slightly lower percentage reduction in THD, highlighting the efficacy of the MSMC in enhancing THD values. Additionally, the amplitude value also decreased significantly from the first test to the second test across both algorithms, indicating that the shape of the waveform considerably impacts the amplitude of the FS at 50 Hz.

Table 4. Variation in current THD and FS (50 Hz) amplitude between the second and first tests.

Amplitude of FS and THD		**MSMC technique**	**Designed technique**
Amplitude of FS (50 Hz)	Test 1	843 A	842.80 A
	Test 2	2386 A	2386 A
	Test 2 – Test 1	+1543	+1543.20
	Ratios (%)	+64.67	+64.68
THD (%)	Test 1	0.84	0.48
	Test 2	0.30	0.18
	Test 2 – Test 1	-0.54	-0.30
	Ratios (%)	-64.29	-62.50

The difference in amplitude values between the two tests was estimated at 36 A for both algorithms, which experienced the same reduction in amplitude. The percentage decrease in amplitude was estimated at 3.28 % for the two robust algorithms. Although the percentage of decrease is small, it indicates that there is an impact. The percentage changes in the amplitude and THD values obtained between the first and second tests are represented graphically in Figure 24. Table 3 and Figure 24 demonstrate that the shape of the WS variation has a significant impact on the value of both THD and the amplitude of the FS (50 Hz). Therefore, it is good to obtain good values for THD. A WS must be used in the advanced steps of varying WSs.

5.3 Test 3

This test differs from previous ones in that it evaluates the efficiency and effectiveness of the new algorithm under varying DFIG parameters. The same WS used in the second test is employed here. In this test, the resistance values are doubled, while the inductance values are halved. The results are presented in Figure 25 and Table 5.

Figure 25a illustrates the *Ps* for both robust controllers. It is evident that this energy closely follows the reference values for both controllers, despite the changes in DFIG parameters. The power takes on negative values and fluctuates in response to variations in WS, exhibiting fast dynamics for both strategies. Figure 25b shows the *Qs* for the two robust algorithms. Even with changes in DFIG parameters, this power continues to track the reference values effectively, even when it reaches zero. Additionally, the *Qs* remain unchanged with variations in WS.

Figure 25c depicts the torque variations over time for both robust methods. This torque also takes negative values, indicating energy generation, and ripples can be observed at the torque level. These fluctuations are more pronounced when using the MSMC compared to the new algorithm. Furthermore, the torque variation pattern mirrors the WS change pattern. Figure 25d illustrates the current fluctuations over time for both controls. The current continually changes in response to the WS variations, maintaining a sinusoidal shape for both controls. The fineness of the current is higher when employing the robust FONMSMC compared to the MSMC.

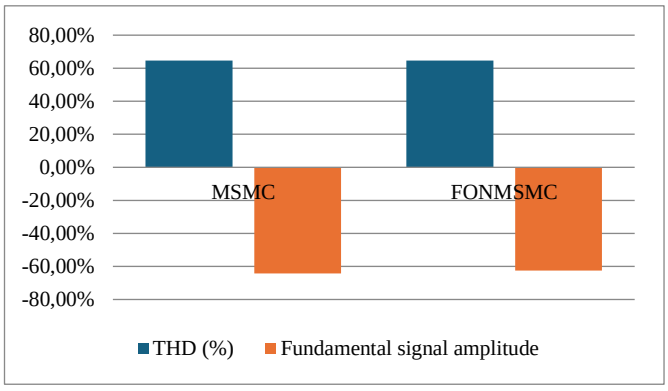

Fig. 24. The ratio changes of both the amplitude and the THD between the tests 1 and 2.

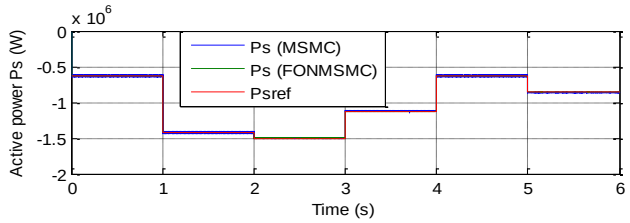

a) *Ps*.

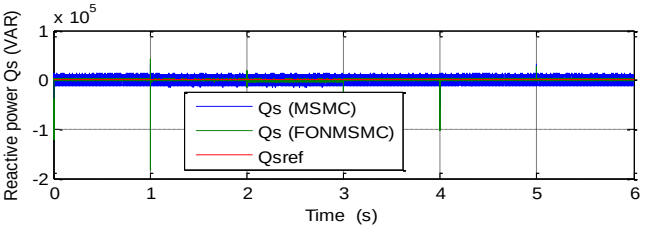

b) *Qs*.

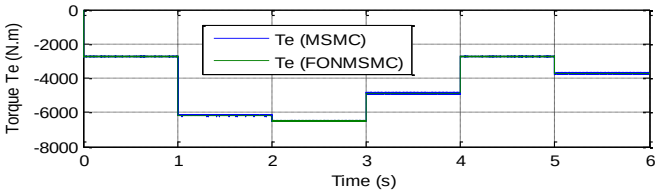

c)Torque.

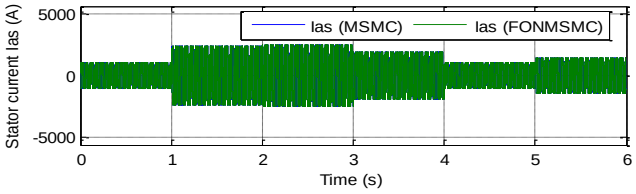

d) Stator current.

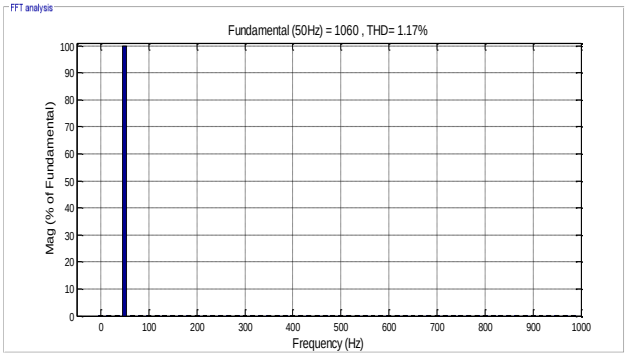

e) Current THD (MSMC).

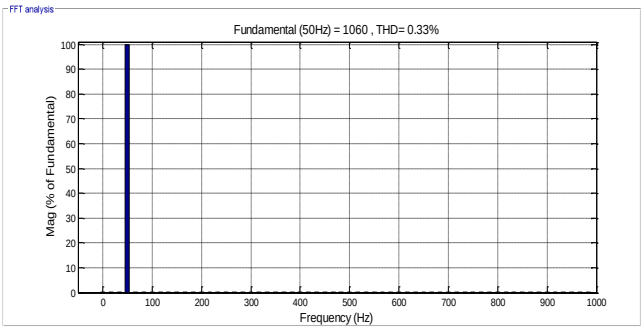

f) Current THD (FONMSMC).

Fig. 25. Test 3 results.

Figures 25e and 25f illustrate the THD of the current values for two different regulators. According to these figures, the THD was found to be 0.33% for the FONMSMC and 1.17% for the MSMC. This indicates that the robust FONMSMC significantly diminishes the THD compared to the MSMC, achieving a reduction of 71.79%. This reduction suggests a higher quality of current when using the FONMSMC. Additionally, both controls operate at the same FS of 50 Hz. In this test, the amplitude value for both methods were estimated to be 1060 A.

Figure 26 illustrates the results of test 3 for both techniques in a zoomed-in view. From this figure, it can be observed that the fluctuations in current, torque, and energy for the DFIG are significantly lower when using the robust FONMSMC compared to the MSMC. These findings demonstrate the efficacy and robustness of the new robust algorithm in enhancing the fineness of power, current, and torque, leading to improved operational performance.

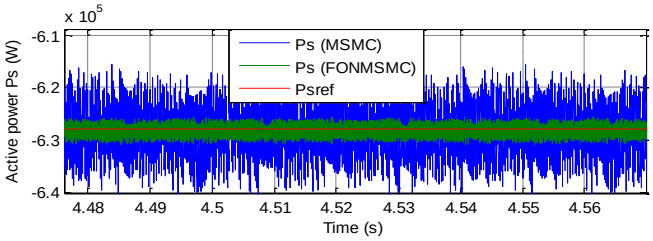

a) *Ps*.

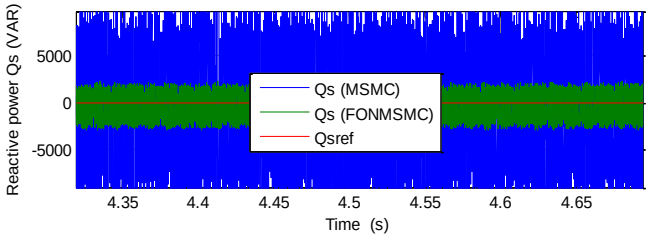

b) *Qs*.

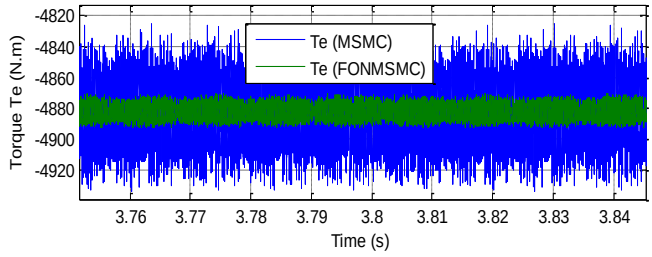

c) Torque.

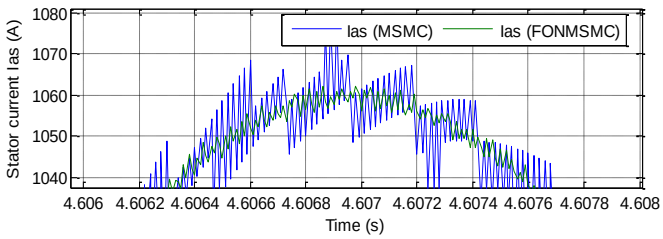

d) Stator current.

Fig. 26. Zoom in the third test results.

Table 5. Reduction rates in the test 3.

Strategies and ratios (%)		***Qs* (VAR)**	***Ps* (W)**
MSMC	Fluctuations	25000	25000
	Overshoot	2782.60	400
	SSE	11374	13170
	RT (ms)	0.055	0.50
FONMSMC	Fluctuations	4000	3200
	Overshoot	1200	600
	SSE	1445.33	2400
	RT (ms)	1.96	1.94
Improvement Ratios (%)	Fluctuations	84 %	87.20 %
	Overshoot	56.87 %	-33.33 %
	SSE	87.29 %	81.78 %
	RT(ms)	-97.19 %	-74.23 %

Table 5 presents the numerical values from test 3, comparing two strategies: robust FONMSMC and MSMC. The table includes values and percentages indicating the reduction in RT, fluctuations, overshoot, and SSE. It demonstrates that the robust FONMSMC outperforms the MSMC in terms of undulations, overshoot, and SSE of DFIG power. For the Qs, the robust FONMSMC achieves reductions in ripples, SSE, and overshoot of 84%, 87.29%, and 56.87%, respectively, compared to the MSMC. In terms of Ps, the FONMSMC minimizes the ripples and SSE by 87.20% and 81.78%, respectively, in comparison to the MSMC.

These decreased rates from test 3 are illustrated graphically in Figure 27, highlighting the superior performance of the robust FONMSMC over the MSMC. However, it should be noted that the robust FONMSMC yielded unsatisfactory results for RT and the overshoot value of *Ps* when compared to the MSMC. This shortcoming may be linked to the gain settings of the robust FONMSMC. Potential improvements could be explored in the future by employing the GWO to determine optimal gain values.

Table 6 presents a study on how the THD of the current and the amplitude of the FS (50 Hz) were affected by both algorithms between tests 2 and 3. From the data in Table 6, it is evident that the THD increased in test 3 compared to the second test for both cases. This indicates that variations in the DFIG parameter values directly influence the THD value.

Specifically, when using the robust FONMSMC, the THD in test 3 rose by 45.45% compared to the second test. In contrast, when employing the MSMC, the THD value increased by 74.36%. This demonstrates that the robust FONMSMC performed better in maintaining a lower THD value despite the variations in DFIG parameters, suggesting that this technique is less impacted by parameter variations than the MSMC.

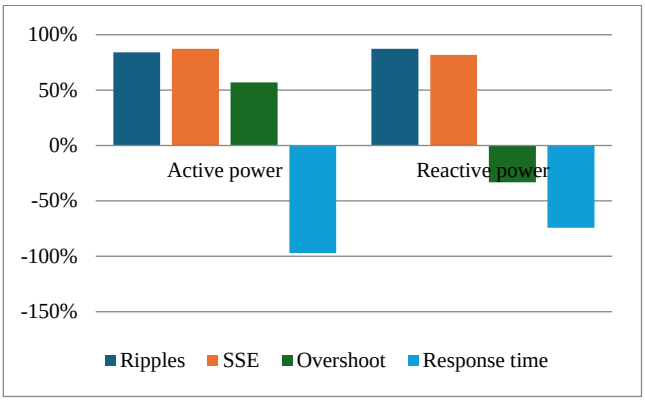

Fig.27. Graphical representation of the minimization ratios in the third test case.

Table 6. Study of the variation in values of current THD and FS (50 Hz) amplitude between the third and first tests.

Amplitude of FS and THD		MSMC technique	Designed technique
Amplitude of FS (50 Hz)	Test 2	2386 A	2386 A
	Test 3	1060 A	1060 A
	Test 3 – Test 2	-1326 A	-1326 A
	Ratios (%)	-55.57	-55.57
THD (%)	Test 2	0.30	0.18
	Test 3	1.17	0.33
	Test 3 – Test 2	+0.87	+0.15
	Ratios (%)	+74.36	+45.45

A decrease in the amplitude value was observed in test 3 relative to test 2 for both control techniques. This reduction, estimated at 55.57%, is attributed to the changes in DFIG parameters, indicating that the amplitude value is negatively influenced by these alterations. The influence ratios of amplitude of the FS (50 Hz) and current THD between tests 1 and 3 are illustrated in Figure 28.

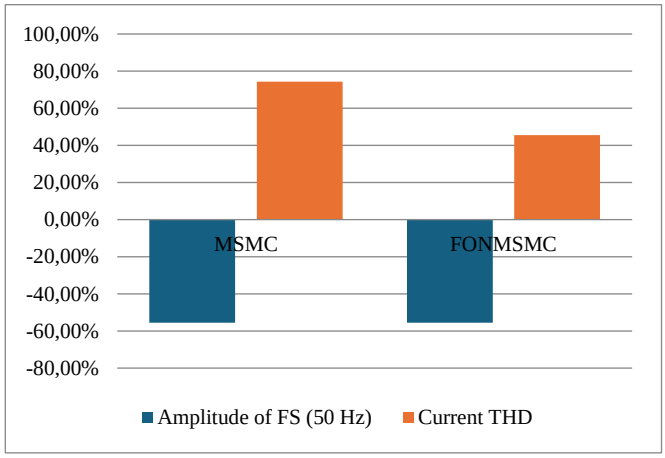

Fig. 28. Graphical representation of the effect ratios of the amplitude and THD values between the tests 3 and 1.

5.4 Test 4: Without MPPT Technique

In this test, we examine the behavior of the new algorithm without using the MPPT, with the reference power (*Ps*) set to a constant value of 1 MW. The results are illustrated in Figures 29 and 30, with numerical data presented in Table 7. Figure 29a shows the variation of *Qs* over time for both controllers. *Qs* remains within the reference value despite fluctuations, and both control methods exhibit a rapid DR. Figure 29b illustrates the variation in *Ps* for the two control techniques, also without the MPPT. The power maintains a close alignment with the reference, showcasing a rapid DR. Additionally, fluctuations are observed in this power level, including instances where the value becomes negative, indicating that the generator is supplying power to the grid.

Figure 29c depicts the variation in torque for the two robust algorithms. It is evident that the torque values mirror the variations observed in *Ps*, even in the absence of the MPPT. Similar fluctuations are present in the torque levels when employing both controls, and negative values are recorded, consistent with findings from previous tests. Figure 29d presents the changes in current over time for the two algorithms. The current follows a sinusoidal pattern with fluctuations, reflecting the observations made in earlier tests. Moreover, it is highlighted that the current values are closely related to those of *Ps*.

Figures 29e and 29f illustrate the THD of current for two control strategies when the MPPT is not implemented. The THD values for the MSMC and the robust FONMSMC are 0.40% and 0.19%, respectively. This indicates that the robust FONMSMC achieves a 52.50% reduction in THD compared to the MSMC. Additionally, both algorithms deliver the same FS (50 Hz) amplitude. These results demonstrate that the robust FONMSMC exhibits superior operational performance compared to the DPC-MSMC, making it a reliable solution for industrial applications. Figure 30 illustrates the results from the fourth test conducted using the Zoom method. The data shows that the fluctuations observed in this test are significantly lower when employing the robust FONMSMC compared to the MSMC. Notably, the robust FONMSMC, despite not utilizing the MPPT, demonstrated highly satisfactory outcomes in terms of torque, power, and current ripples.

In this test, the estimated current ripples were measured at 14 A for the MSMC and only 2.65 A for the FONMSMC. This indicates that the robust FONMSMC diminishes the current undulation by an impressive 81.07% compared to the MSMC. Similarly, torque undulations were estimated at 40 N·m for MSMC and 6.76 N·m for FONMSMC. Thus, the robust FONMSMC achieved a minimization of 83.10% in torque undulation relative to the MSMC. Moreover, the Ps fluctuations were estimated at 9900 W for the MSMC and 2000 W for the DPC- robust FONMSMC, reflecting a reduction of 79.80% when using the robust FONMSMC. Additionally, the Qs fluctuations were estimated at 12293.39 VAR for the MSMC and 2343.80 VAR for the robust FONMSMC, resulting in an 80.93% reduction in Qs fluctuations with the robust FONMSMC as compared to MSMC.

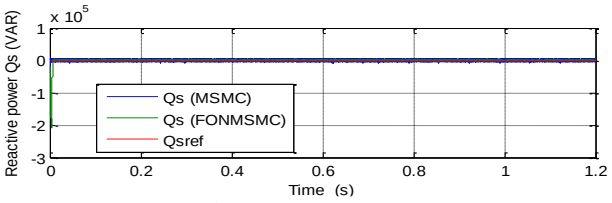

a) Reactive power.

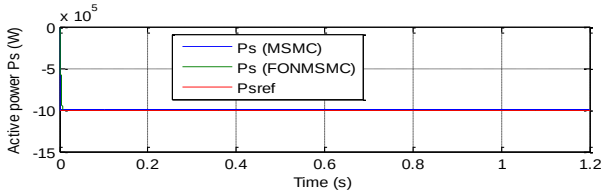

b) Active power.

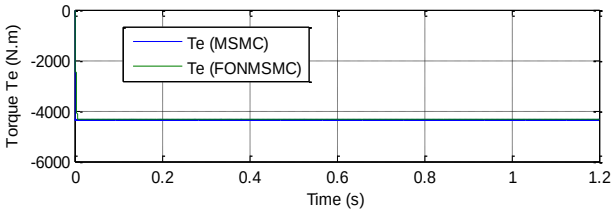

c) Torque.

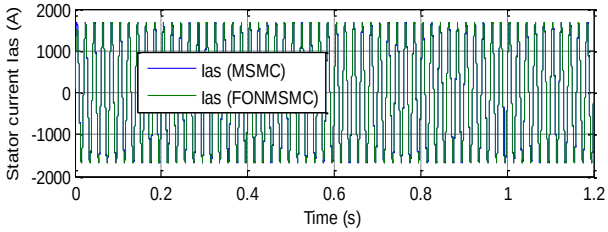

d) Current I_{as}.

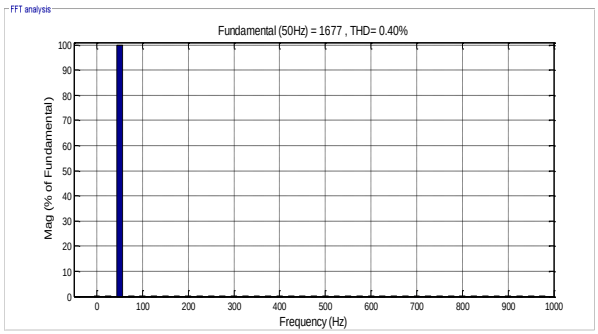

e) THD (MSMC).

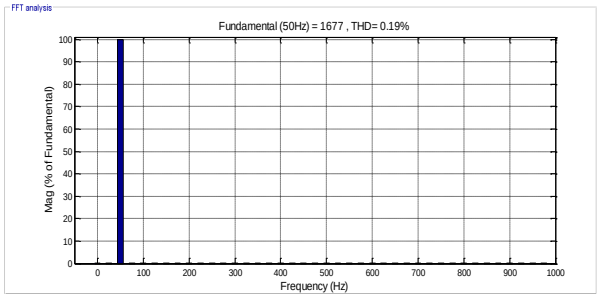

f) THD (FONMSMC).

Fig. 29. Fourth test results.

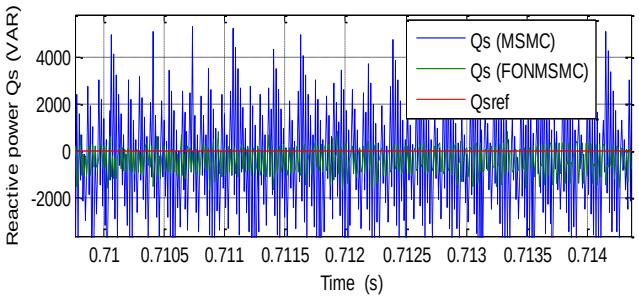

a) Reactive power.

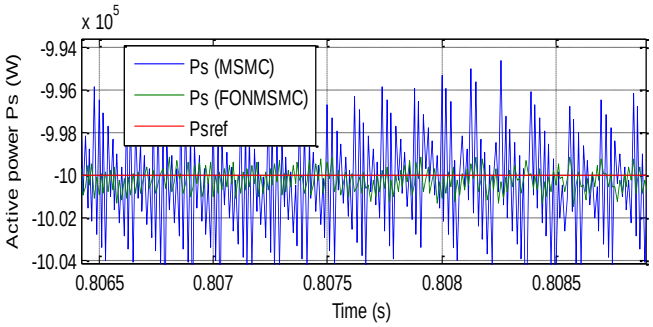

b) Active power.

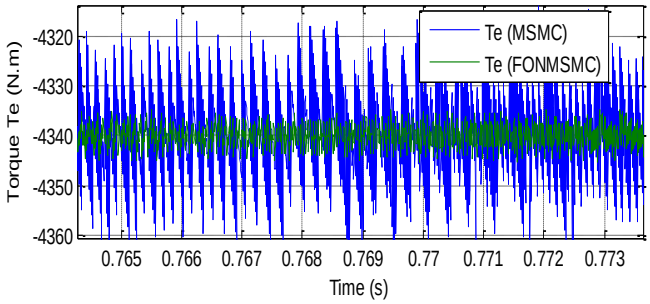

c) Torque.

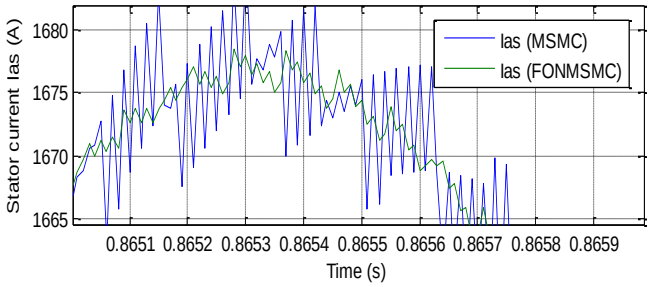

d) Current I_{as}.

Fig. 30. Zoom in the fourth test results.

Figure 31 displays the ripple minimization ratios achieved in the fourth test in relation to the MSMC. This figure clearly illustrates the superiority of the new algorithm and its significant capacity to enhance the quality of current and power, making it a promising solution in various fields.

Table 7 presents the numerical results for two methods that do not utilize the MPPT. The findings indicate that the FONMSMC delivered significantly better results compared to the MSMC. Specifically, the overshoot values for both the Ps and Qs were reduced by 88.65% and 23.08%, respectively, when using the robust FONMSMC.

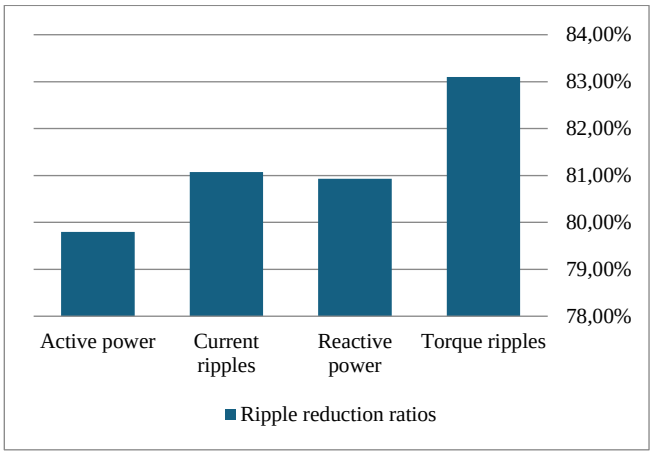

Fig. 31. Graph of ripple reduction ratios in the fourth test.

Table 7. Ratios of overshoot, RT, and SSE of both algorithms in the test4.

Methods and ratios (%)		***Qs* (VAR)**	***Ps* (W)**
MSMC	Overshoot	3083.50	1300
	SSE	1278	6000
	RT (ms)	1.57	1.57
FONMSMC	Overshoot	350	1000
	SSE	224	360
	RT **(**ms**)**	6.30	6.30
Ratios (%)	Overshoot	88.65	23.08
	SSE	82.47	94
	RT **(**ms**)**	-75.08	-75.08

Additionally, the robust FONMSMC achieved a reduction in the SSE of 82.47% for Ps and 94% for *Qs* compared to the MSMC. These results clearly demonstrate the superior operational performance of the robust FONMSMC over the other algorithms. Figure 32 illustrates the percentage reductions achieved in test 4 when compared to the MSMC. This figure emphasizes that RT is a significant drawback of the regulator designed in this study. This issue is attributed to the gain values of the new regulator. However, this drawback could potentially be addressed in the future by integrating the new robust algorithm with other strategies, such as GAs.

Table 8 illustrates a study examining the changes in amplitude and THD values between the second and fourth tests using two different approaches. The data indicate that the amplitude value decreased in the fourth test compared to the second for both techniques, with a reduction estimated at 29.72%. This decline can be attributed to the lack of the MPPT in the fourth test. In contrast, the THD significantly increased in the fourth test relative to the second test for both controllers. This indicates that the absence of the MPPT has a considerable impact on the THD. Specifically, the increase in THD was estimated at 25% for the MSMC and 5.26% for the robust FONMSMC. The influence ratios observed between the second and fourth tests are illustrated in Figure 33.

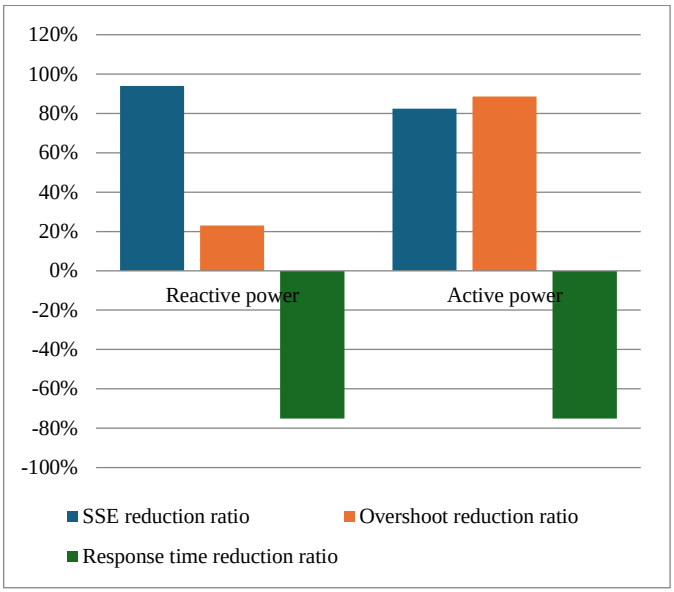

Fig. 32. Graph of reduction ratios in the fourth test.

Table 8. Study of the variation in values of current THD and FS (50 Hz) amplitude between the second and fourth tests.

Amplitude of FS and THD		**MSMC technique**	**Designed technique**
Amplitude of FS (50 Hz)	Test 2	2386 A	2386 A
	Test 4	1677 A	1677 A
	Test 4 – Test 2	+709 A	+709 A
	Ratios (%)	+29.72	+29.72
THD (%)	Test 2	0.30	0.18
	Test 4	0.40	0.19
	Test 4 – Test 2	+0.10	+0.01
	Ratios (%)	+25	+5.26

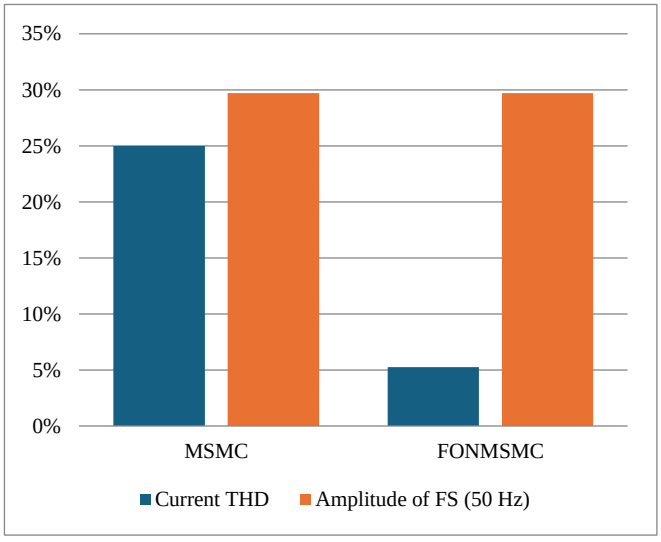

Fig. 33. Graph of percentage change in amplitude and THD values between the tests 4 and 1.

From these ratios, it is clear that the robust FONMSMC demonstrated a significantly lower impact on THD compared to the MSMC. This finding highlights the strength and efficacy of the robust FONMSMC in enhancing current characteristics and the overall performance of the control ES. These promising results suggest that this new algorithm may be of interest for future applications in various industrial settings.

Finally, the new algorithm is compared with related works regarding THD values. Table 9 illustrates this comparison, showing that the robust FONMSMC achieves significantly better THD values than several other strategies, including the SMC (2.56%), DPC-STC (1.66%), and SOSMC (3.13%). In all tests, the robust FONMSMC consistently outperformed numerous studies, making it a promising candidate for future industrial applications. Table 9 underscores the efficacy and strength of the new algorithm in enhancing performance compared to various methods, such as DTC-PI, integral SMC, and type 2 FL control-based FOC techniques.

Table 9. Comparison in terms of current THD.

References	**Algorithms**		**THD (%)**
[77]	High-order SMC		1.08
	SMC		2.56
[78]	FOC		3.7
	T2FLC-FOC		1.14
[79]	DPC-STC		1.66
[80]	DTC		2.57
[81]	Fuzzy-SMC		1.15
[82]	Second-order SMC		3.13
[83]	Power control	Method 1	5.6817
		Method 2	3.1873
[84]	DTC		8.75
	3-level DTC		1.57
[85]	DTC-PI		12
	DTC-ACO		7.19
[86]	SMC based on multi-resonant algorithm		3.14
	Integral SMC		9.71
[44]	Direct FOC		2.94
	Improved direct FOC		1.42
[87]	Direct FOC		1.45
DPC-FONMSMC	0.64		
	1.25		
	0.12		
	0.19		

A comparison was made in Tables 10 and 11 with related studies regarding fluctuation diminutive ratios and the SSE value of DFIG energy. The results indicate that the new algorithm achieved significantly higher minimization rates for both ripple and SSE compared to several related studies.

In Table 10, which presents the results from the first test of the new robust algorithm, the ripple value reductions for Ps were 28.46%, 63.93%, 12.46%, and 87.37% when compared to the studies referenced as [88], [93], [90], and [95], respectively.

Table 11, on the other hand, shows that the new algorithm resulted in SSE of Ps reduction ratios of 68.76%, 38.53%, 61.58%, and 49.69% for the same studies [88], [93], [90], and [95]. Additionally, the approach demonstrated better SSE minimization ratios for *Qs* compared to studies [89], [93], and [95] by 48.05%, 38.30%, and 31.39%, respectively.

These comparisons underscore the efficiency and strength of the new algorithm in enhancing PQ compared to various works. Furthermore, the ability of the new robust algorithm to enhance SSE values positions it as a promising area for future research.

Table 10. Comparison with related works in terms of ripples diminutive ratio of DFIG power.

References	**Ratios (%)**	
	***Qs* (KVA)**	***Ps* (W)**
[88]	54.25	56.66
	46.68	47.50
	50.74	50.41
[89]	35	36
[90]	47.05	69.33
	47.99	65.07
[91]	36.93	22.95
[92]	20.66	37.50
	20.80	16.66
[93]	46.93	28.57
[94]	50	44.50
	52.98	63.33
	50	48.18
[95]	12.02	10
	10.53	5.88
Proposed approach	85.90	79.20
	80	83.20
	87.20	84
	80.93	79.80

Table 11. Comparison with related studies in terms of SSE strength ratio of DFIG energy.

References	SSE ratios (%)	
	***Qs* (VAR)**	***Ps* (W)**
[92]	76.55	28.76
	24.62	30.48
[93]	42.14	47.57
[40]	38.32	50
	39.68	40
[95]	46.86	63.96
	45.48	78
	43.21	60.03
[91]	36.93	35
[89]	35.48	62
[88]	78.44	45.83
	52.22	56.52
	48.75	87.50
Proposed technique	68.30	91.10
	90	95.60
	87.29	81.78
	82.47	94

6. Conclusions

This work introduced a fractional-order neural modified sliding mode control (FONMSMC) strategy for dual-rotor wind turbines employing doubly fed induction generators (DFIGs) to address challenges in power quality, harmonic distortion, and system robustness. By combining fractional calculus, neural adaptation, and a modified SMC framework, the proposed controller achieved notable performance gains, including a 71.79% reduction in THD, 87.2% cleaner active power, and a 94% decrease in steady-state error, outperforming conventional DPC-MSMC and other advanced methods. These results demonstrate enhanced grid stability, reduced maintenance costs, and greater operational reliability.

Future work will focus on experimental validation, hardware-in-the-loop implementation, and adaptive optimization to confirm industrial applicability. Extending the approach to multi-turbine coordination and exploring fault-tolerant and cyber-secure designs will further support its deployment in next-generation smart grid and renewable energy systems.

Nomenclature

NN	Neural network
DPC	Direct power control
SMC	Sliding mode control
PI	Proportional-integral controller
THD	Total harmonic distortion
WS	Wind speed
WE	Wind energy
DFIG	Doubly-feed induction generator
SSE	Steady-state error
FL	Fuzzy logic
MPPT	Maximum power point tracking
MSMC	Modified sliding mode control
STA	Super-twisting algorithm
Ps	Active power
Qs	Reactive power
SOSMC	Second-order sliding mode control
FONMSMC	Fractional-order modified sliding mode control

Author Contributions

H.B. was responsible for the conceptualization, validation, resources, data curation, software development, and project administration. H.B. and N.B. jointly contributed to the methodology, formal analysis, investigation, original draft preparation, review and editing, visualization, supervision, and funding acquisition. All authors have read and agreed to the published version of the manuscript.

Conflict of Interest:

The author(s) declared no potential conflicts of interest with respect to the research, authorship, and/or publication of this article.

References

[1] M. K. Senapati, C. Pradhan, S. Ranjan Samantaray, P. K. Nayak, "Improved power management control strategy for renewable energy-based DC micro-grid with energy storage integration," IET Generation, Transmission and Distirbution vol. 13, no. 6, pp. 838-849, 2019. https://doi.org/10.1049/iet-gtd.2018.5019.

[2] M. K. Senapati, C. Pradhan, P. K. Nayak, S. R. Samantaray, "Lagrange interpolating polynomial–based deloading control scheme for variable speed wind turbines," International Transaction on Electrical Energy Systems In Press, 2019. https://doi.org/10.1002/2050-7038.2824.

[3] M. K. Senapati, O. Al Zaabi, K. Al Hosani, K. Al Jaafari, C. Pradhan, U. Ranjan Muduli, "Advancing Electric Vehicle Charging Ecosystems with Intelligent Control of DC Microgrid Stability," In IEEE Transactions on Industry Applications vol. 60, no. 5, pp. 7264-7278, 2024. Doi: 10.1109/TIA.2024.3413052.

[4] Z. -C. Zou, X. -Y. Xiao, Y. -F. Liu, Y. Zhang and Y. -H. Wang, "Integrated Protection of DFIG-Based Wind Turbine With a Resistive-Type SFCL Under Symmetrical and Asymmetrical Faults," in IEEE Transactions on Applied Superconductivity, vol. 26, no. 7, pp. 1-5, Oct. 2016, Art no. 5603005, doi: 10.1109/TASC.2016.2574352.

[5] D. Somnath, A. K. Akella, "Power Flow Control of PV-Wind-Battery Hybrid Renewable Energy Systems for Stand-Alone Application," Int. J. Renew. Energy Res 2018, https://doi.org/10.20508/ ijrer.v8i1.6534.g7278.

[6] S. Wang, J. Hu and X. Yuan, "Virtual Synchronous Control for Grid-Connected DFIG-Based Wind Turbines," in IEEE Journal of Emerging and Selected Topics in Power Electronics, vol. 3, no. 4, pp. 932-944, Dec. 2015, doi: 10.1109/JESTPE.2015.2418200.

[7] J. Mohammadi, S. Vaez-Zadeh, S. Afsharnia and E. Daryabeigi, "A Combined Vector and Direct Power Control for DFIG-Based Wind Turbines," in IEEE Transactions on Sustainable Energy, vol. 5, no. 3, pp. 767-775, July 2014, doi: 10.1109/TSTE.2014.2301675.

[8] M. C. Bueso, A. Molina-García, A. P. Ramallo-González and A. Fernández-Guillamón, "Characterization of Vertical Wind Speed Profiles Based on Ward's Agglomerative Clustering Algorithm," in Journal of Modern Power Systems and Clean Energy, vol. 11, no. 5, pp. 1437-1449, September 2023, doi: 10.35833/MPCE.2022.000703.

[9] J. Xie, X. Zhang, S. Huang, F. Huang, Z. Peng, Y. Dai, X. Wu, "Characteristics Simulation Method of Megawatt Three-Blade Horizontal Axis Wind Turbine Based on Laboratory Kilowatt Low-Power Motor System," in IEEE Transactions on Industry Applications, vol. 58, no. 1, pp. 645-655, Jan.-Feb. 2022, doi: 10.1109/TIA.2021.3123116.

[10] Z. –C. Zou, X. –Y. Xiao, Y. –F. Liu, Y. Zhang, Y. –H. Wang, "Integrated Protection of DFIG-Based Wind Turbine with a Resistive-Type SFCL Under Symmetrical and Asymmetrical Faults," In IEEE Transactions on Applied Superconductivity vol. 26, no. 7, pp. 1-5, 2016. Doi: 10.1109/TASC.2016.2574352.

[11] K. -J. Du, X. -P. Ma, Z. -X. Zheng, C. -S. Li, W. -X. Hu and K. -S. Dong, "LVRT Capability Improvement of DFIG-Based Wind Turbines With a Modified Bridge-Resistive-Type SFCL," in IEEE Transactions on Applied Superconductivity, vol. 31, no. 8, pp. 1-5, Nov. 2021, Art no. 5603005, doi: 10.1109/TASC.2021.3091114.

[12] X. -Y. Xiao, R. -H. Yang, Z. -X. Zheng and Y. Wang, "Cooperative Rotor-Side SMES and Transient Control for Improving the LVRT Capability of Grid-Connected DFIG-Based Wind Farm," in IEEE Transactions on Applied Superconductivity, vol. 29, no. 2, pp. 1-5, March 2019, Art no. 0600204, doi: 10.1109/TASC.2018.2881315.

[13] H. Zhou, P. Ju, Y. Xue and J. Zhu, "Probabilistic equivalent model of DFIG-based wind farms and its application in stability analysis," in Journal of Modern Power Systems and Clean Energy, vol. 4, no. 2, pp. 248-255, April 2016, doi: 10.1007/s40565-015-0156-5.

[14] X. Zou, D. Zhu, J. Hu, S. Zhou and Y. Kang, "Mechanism Analysis of the Required Rotor Current and Voltage for DFIG-Based WTs to Ride-Through Severe Symmetrical Grid Faults," in IEEE Transactions on Power Electronics, vol. 33, no. 9, pp. 7300-7304, Sept. 2018, doi: 10.1109/TPEL.2018.2799218.

[15] Z. Fan, G. Song, X. Kang, J. Tang and X. Wang, "Three-phase fault direction identification method for outgoing transmission line of DFIG-based wind farms," Journal of Modern Power Systems and Clean Energy, vol. 7, no. 5, pp. 1155-1164, September 2019, doi: 10.1007/s40565-018-0485-2.

[16] I. Villanueva, A. Rosales, P. Ponce and A. Molina, "Grid-Voltage-Oriented Sliding Mode Control for DFIG Under Balanced and Unbalanced Grid Faults," IEEE Transactions on Sustainable Energy, vol. 9, no. 3, pp. 1090-1098, July 2018, doi: 10.1109/TSTE.2017.2769062.

[17] N. Ullah, M. Asghar Ali, A. Ibeas, J. Herrera, "Adaptive Fractional Order Terminal Sliding Mode Control of a Doubly Fed Induction Generator-Based Wind Energy System," IEEE Access vol. 5, pp. 21368-21381, 2017. Doi: 10.1109/ACCESS.2017.2759579.

[18] X. Zhu, S. Liu and Y. Wang, "Second-order sliding-mode control of DFIG-based wind turbines," 3rd Renewable Power Generation Conference (RPG 2014), Naples, 2014, pp. 1-6, doi: 10.1049/cp.2014.0936.

[19] B. Bossoufi, M. Karim, M. Taoussi, H. A. Aroussi, M. Bouderbala, O. Deblecker, S. Motahhir, A. Nayyar, M. A. Alzain, "Rooted Tree Optimization for the Backstepping Power Control of a Doubly Fed Induction Generator Wind Turbine: dSPACE Implementation," in IEEE Access, vol. 9, pp. 26512-26522, 2021, doi: 10.1109/ACCESS.2021.3057123.

[20] X. Yu, Z. Jiang and Y. Zhang, "A synergetic control approach to grid-connected, wind-turbine doubly-fed induction generators," 2008 IEEE Power Electronics Specialists Conference, Rhodes, Greece, 2008, pp. 2070-2076, doi: 10.1109/PESC.2008.4592248.

[21] S. Rajendran, D. Jena, M. Diaz, J. Rodríguez, "Terminal Integral Synergetic Control for Wind Turbine at Region II Using a Two-Mass Model," Processes vol. 11, pp. 616, 2023. https://doi.org/10.3390/pr11020616.

[22] M. R. Islam, J. Hasan, M. R. R. Shipon, M. A. H. Sadi, A. Abuhussein and T. K. Roy, "Neuro Fuzzy Logic Controlled Parallel Resonance Type Fault Current Limiter to Improve the Fault Ride Through Capability of DFIG Based Wind Farm," IEEE Access, vol. 8, pp. 115314-115334, 2020, doi: 10.1109/ACCESS.2020.3000462.

[23] M. Samir, H. Mohamed, K. Nadir, K. Selman, "Neural Network Based Field Oriented Control for Doubly Fed Induction Generator," International Journal of Smart Grid, vol. 2, no. 3, pp. 183-187, 2018. https://doi.org/10.20508/ijsmartgrid.v2i3.18.g18.

[24] L. Djilali, A. Badillo-Olvera, Y. Yuliana Rios, H. López-Beltrán, L. Saihi, "Neural High Order Sliding Mode Control for Doubly Fed Induction Generator based Wind

Turbines," IEEE Latin America Transactions vol. 20, no. 2, pp. 223-232, 2022. Doi: 10.1109/TLA.2022.9661461.

[25] I. Sami, S. Ullah, S. U. Amin, A. Al-Durra, N. Ullah and J. Ro, "Convergence Enhancement of Super-Twisting Sliding Mode Control Using Artificial Neural Network for DFIG-Based Wind Energy Conversion Systems," In IEEE Access, vol. 10, pp. 97625-97641, 2022. Doi: 10.1109/ACCESS.2022.3205632.

[26] A. Darvish Falehi, H. Torkaman, "Promoted supercapacitor control scheme based on robust fractional-order super-twisting sliding mode control for dynamic voltage restorer to enhance FRT and PQ capabilities of DFIG-based wind turbine," Journal of Energy Storage vol. 42, pp. 102983, 2021. https://doi.org/10.1016/j.est.2021.102983.

[27] Y. L. A. Sumanth L. Lakshminarasimman, R. G. Sambasiva, "Optimal design of FoPID controller for DFIG based wind energy conversion system using Grey-Wolf optimization algorithm," Int'l Journal of Renewable Energy Research vol. 12, no. 4, pp. 2111-2120, 2022. Doi: 10.20508/ijrer.v12i4.13446.g8594.

[28] N. Khosravi, S. Echalih, Z. Hekss, R. Baghbanzadeh, M. Messaoudi, M. Shahideipour, "A New Approach to Enhance the Operation of M-UPQC Proportional-Integral Multiresonant Controller Based on the Optimization Methods for a Stand-Alone AC Microgrid," In IEEE Transactions on Power Electronics vol. 38, no. 3, pp. 3765-3774, 2023. Doi: 10.1109/TPEL.2022.3217964.

[29] K. Nima, "Enhancing operational efficiency through a control-based approach for hydrogen and battery energy storage systems integration in renewable energy networks," Renewable Energy vol. 248, pp. 123132, 2025. https://doi.org/10.1016/j.renene.2025.123132.

[30] A. Darvish Falehi, "Optimal robust disturbance observer based sliding mode controller using multi-objective grasshopper optimization algorithm to enhance power system stability. J Ambient Intell Human Comput vol. 11, pp. 5045–5063, 2020. https://doi.org/10.1007/s12652-020-01811-8.

[31] F. A. Darvish, "An innovative optimal RPO-FOSMC based on multi-objective grasshopper optimization algorithm for DFIG-based wind turbine to augment MPPT and FRT capabilities," Chaos, Solitons & Fractals vol. 130, pp. 109407, 2020. https://doi.org/10.1016/j.chaos.2019.109407.

[32] K. Nima, R. A. Hamid, "A hierarchical deep learning-based recurrent convolutional neural network for robust voltage and frequency operation management in microgrids," Applied Soft Computing vol. 170, pp. 112645, 2025. Doi: 10.1016/j.asoc.2024.112645.

[33] K. Nima, "Finite-Time control scheme for effective voltage and frequency regulation in networked microgrids. International Journal of Electrical Power & Energy Systems vol. 165, pp. 110481, 2025. https://doi.org/10.1016/j.ijepes.2025.110481.

[34] H. Jeong, W. Kim, K. Lee, Byung-Chang Jeong and Seung-Ho Song, "A sliding-mode approach to control the active and reactive powers for A DFIG in wind turbines," 2008 IEEE Power Electronics Specialists Conference, Rhodes, 2008, pp. 120-125, doi: 10.1109/PESC.2008.4591910.

[35] N. Ullah, I. Sami, M. S. Chowdhury, K. Techato and H. I. Alkhammash, "Artificial Intelligence Integrated Fractional Order Control of Doubly Fed Induction Generator-Based Wind Energy System," in IEEE Access, vol. 9, pp. 5734-5748, 2021, doi: 10.1109/ACCESS.2020.3048420.

[36] F. Boucetta, M. Alturki, A. Albaker, K. Alqunun, M. T. Benchouia, B. M. Alshammari, M. Becherif, T. Guesmi, "Robust direct voltage control of stand-alone DFIG wind systems using a fractional-order fuzzy logic approach," Sci Rep vol. 15, pp. 28762, 2025. https://doi.org/10.1038/s41598-025-11910-1.

[37] B. Habib, "Fractional-order synergetic control of the asynchronous generator-based variable-speed multi-rotor wind power systems," IEEE Access vol. 11, pp. 133490-133508, 2024. Doi: 10.1109/ACCESS.2023.3335902.

[38] H. Benbouhenni, G. Hamza, M. Oproescu, N. Bizon, P. Thounthong, I. Colak, "Application of fractional-order synergetic-proportional integral controller based on PSO algorithm to improve the output power of the wind turbine power system," Sci. Rep. vol. 14, pp. 609, 2024. https://doi.org/10.1038/s41598-024-51156-x.

[39] B. Habib, I. Laurentiu-Mihai, M. Alin-Gheorghita, D. Zellouma, I. Colak, N. Bizon, "Active and reactive power vector control using neural-synergetic-super twisting controllers of induction generators for variable-speed contra-rotating wind turbine systems," Measurement and Control vol. 57, no. 7, pp. 919-948, 2024. doi:10.1177/00202940231224386.

[40] M. Yessef, B. Habib, M. Taoussi, A. Lagrioui, I. Colak, S. Mobayen, A. Zhilenkov, B. Bossoufi, "Real-time validation of intelligent super twisting sliding mode control for variable-speed DFIG using dSPACE 1104 board," In IEEE Access vol. 12, pp. 31892-31915, 2024. Doi: 10.1109/ACCESS.2024.3367828.

[41] H. Gasmi, B. Habib, S. Mendaci, I. Colak, "A new scheme of the fractional-order super twisting algorithm for asynchronous generator-based wind turbine," Energy Reports vol. 9, pp. 6311-6327, 2023. https://doi.org/10.1016/j.egyr.2023.05.267.

[42] B. Habib, I. Colak, N. Bizon, "Application of genetic algorithm and terminal sliding surface to improve the effectiveness of the proportional–integral controller for the direct power control of the induction generator power system," Engineering Applications of Artificial Intelligence vol. 125, pp. 106681, 2023. https://doi.org/10.1016/j.engappai.2023.106681.

[43] B. Habib, H. Gasmi, I. Colak, N. Bizon, P. Thounthong, "Synergetic-PI controller based on genetic algorithm for

DPC-PWM strategy of a multi-rotor wind power system," Scientific Report vol. 13, pp. 13570, 2023. https://doi.org/10.1038/s41598-023-40870-7.

[44] S. Lee, G. Kim, D. Lee, Y. Kwon, "Robust low complexity multisurface super twisting sliding mode control for DFIG systems," Sci Rep 2025. https://doi.org/10.1038/s41598-025-29985-1.

[45] I. Sami, S. Ullah, S. U. Amin, A. Al-Durra, N. Ullah and J. Ro, "Convergence Enhancement of Super-Twisting Sliding Mode Control Using Artificial Neural Network for DFIG-Based Wind Energy Conversion Systems," in IEEE Access, vol. 10, pp. 97625-97641, 2022, doi: 10.1109/ACCESS.2022.3205632.

[46] A. Yahdou, B. Habib, I. Colak, N. Bizon, "Application of Backstepping Control With Nonsingular Terminal Sliding Mode Surface Technique to Improve the Robustness of Stator Power Control of Asynchronous Generator-Based Multi-Rotor Wind Turbine System," Electric Power Components and Systems In Press, pp. 1-19, 2024. DOI: 10.1080/15325008.2024.2304688.

[47] P. Xiong and D. Sun, "Backstepping-Based DPC Strategy of a Wind Turbine-Driven DFIG Under Normal and Harmonic Grid Voltage," in IEEE Transactions on Power Electronics, vol. 31, no. 6, pp. 4216-4225, June 2016, doi: 10.1109/TPEL.2015.2477442.

[48] A. Yahdou, A. B. Djilali, E. Bounadja, H. Benbouhenni, "Using neural network super-twisting sliding mode to improve power control of a dual-rotor wind turbine system in normal and unbalanced grid fault modes," International Journal of Circuit Theory and Applications vol. 52, no. 9, pp. 4323-4347, 2024. https://doi.org/10.1002/cta.3960.

[49] K. H. S⊘renserr, T. Knudsen, O. T. Filsoof, T. G. Hovgaard, J. D. Grunnet, J. X. V. Neto, R. Wisniewski, "Multi-Rotor Wind Turbine Control Challenge - A Benchmark for Advanced Control Development," 2018 IEEE Conference on Control Technology and Applications (CCTA), Copenhagen, Denmark, 2018, pp. 1615-1622, doi: 10.1109/CCTA.2018.8511511.

[50] P. Jamieson, M. Branney, "Structural Considerations of a 20MW Multi-Rotor Wind Energy System," J. Phys. Conf. Ser., Vol. 555, pp. 012013, 2014. https://doi.org/10.1088/1742-6596/555/1/012013.

[51] B. Habib, N. Bizon, "Advanced Direct Vector Control Method for Optimizing the Operation of a Double-Powered Induction Generator-Based Dual-Rotor Wind Turbine System," Mathematics vol. 9, no. 19, pp. 2297, 2021. Doi: 10.3390/math9182297.

[52] F. Mazouz, S. Belkacem, I. Colak, S. Drid, "Direct Power Control of DFIG by Sliding Mode Control and Space Vector Modulation," International Conference on Systems and Control (ICSC), Valencia, Spain, 2018, pp. 462-467. Doi: 10.1109/ICoSC.2018.8587848.

[53] P. P. Pradhan, B. Subudhi and A. Ghosh, "A Robust Multiloop Disturbance Rejection Controller for a Doubly Fed Induction Generator-Based Wind Energy Conversion System," in IEEE Journal of Emerging and Selected Topics in Power Electronics, vol. 10, no. 5, pp. 6266-6273, Oct. 2022, doi: 10.1109/JESTPE.2022.3155561.

[54] S. Kadi, K. Imarazene, B. El Madjid, B. Habib, E. Abdelkarim, "A direct vector control based on modified SMC theory to control the double-powered induction generator-based variable-speed contra-rotating wind turbine systems," Energy Reports vol. 8, pp. 15057–15066, 2022. Doi: 10.1016/j.egyr.2022.11.052.

[55] Y. Mi, Y. Ma, X. He, X. Yang, J. Gong, Y. Zhao, R. Liu, W. Wei, "Robust Load Frequency Control for Isolated Microgrids Based on Double-loop Compensation," in CSEE Journal of Power and Energy Systems, vol. 9, no. 4, pp. 1359-1369, July 2023, doi: 10.17775/CSEEJPES.2020.04800.

[56] E. Yasser, H. S. Naggar, Z. Abdalhalim, "Assessing Wind Energy Conversion Systems Based on Newly Developed Wind Turbine Emulator," Int'l Journal of Smart Grid, vol. 4, no. 4, pp. 139-148, 2020. https://doi.org/10.20508/ijsmartgrid.v4i4.133.g101.

[57] A. Mohammed, E. Ahmed, N. Tamou, C. Haitam, "Comparative Analysis of ADRC & PI Controllers Used in Wind Turbine System Driving a DFIG," International Journal of Renewable Energy Research-IJRER vol. 7, no. 4, pp. 1816-1824, 2017.

[58] B. Tarek, A. S. Islam, K. I. Doaa, "Performance Enhancement of Doubly-Fed Induction Generator-Based-Wind Energy System," Int'l Journal of Renewable Energy Research, vol. 3, no. 1, pp. 311-325, 2023. https://doi.org/10.20508/ijrer.v13i1.13649.g8685.

[59] E. Amira, I. Amr, A. Abdellatif, S. Shaaban, "Aerodynamic Performance and Structural Design of 5 MW Multi Rotor System (MRS) Wind Turbines," International Journal of Renewable Energy Research-IJRER vol. 12, no. 3, pp. 1495-1505, 2022. https://doi.org/10.20508/ijrer.v12i3.13343.g8535.

[60] O. Beik and A. S. Al-Adsani, "Active and Passive Control of a Dual Rotor Wind Turbine Generator for DC Grids," in IEEE Access, vol. 9, pp. 1987-1995, 2021, doi: 10.1109/ACCESS.2020.3047267.

[61] A. Yahdou, B. Hemici, Z. Boudjema, "Sliding mode control of dual rotor wind turbine system," The Mediterranean Journal of Measurement and Control vol. 11, no. 2, pp. 412-419, 2015.

[62] D. V. N. Ananth, G. V. N. Kumar, "Sustainable operation and performance improvement of grid connected DFIG during symmetrical faults using fuzzy controller based enhanced field-oriented control," Cogent Engineering vol. 3, no. 1, pp. 1221593, 2026. https://doi.org/10.1080/23311916.2016.1221593.

[63] H. Benbouhenni, I. Colak, Z.M.S. Elbarbary, "Reducing power ripple for multi-rotor wind energy systems using

FOPDPI controllers," Sci Rep vol. 15, pp. 12524, 2025. https://doi.org/10.1038/s41598-025-96625-z.

[64] H. Benbouhenni, A. Yahdou, A. B. Djilali, "Solving the problem of power ripples for a multi-rotor wind turbine system using fractional-order third-order sliding mode algorithms," Sci Rep vol. 15, pp. 5636, 2025. https://doi.org/10.1038/s41598-025-89636-3.

[65] D. G. Giaourakis, A. N. Safacas, "Effect of Short-Circuit Faults in the Back-to-Back Power Electronic Converter and Rotor Terminals on the Operational Behavior of the Doubly-Fed Induction Generator Wind Energy Conversion System," Machines vol. 3, pp. 2-26, 2015. https://doi.org/10.3390/machines3010002.

[66] O. Beik, A. S. Al-Adsani, "Active and Passive Control of a Dual Rotor Wind Turbine Generator for DC Grids," In IEEE Access vol. 9, pp. 1987-1995, 2021. Doi: 10.1109/ACCESS.2020.3047267.

[67] W. Zhao, T. A. Lipo, B. –I. Kwon, "A novel dual-rotor axial field fault-tolerant flux-switching permanent magnet machine with high-torque performance," IEEE Trans. Magn. Vol. 51, no. 11, pp. 1-4, 2015.

[68] S. S. Xu, C. Chen, Z. Wu, "Study of Nonsingular Fast Terminal Sliding-Mode Fault-Tolerant Control," IEEE Transactions on Industrial Electronics vol. 62, no. 6, pp. 3906-3913, 2015. Doi: 10.1109/TIE.2015.2399397.

[69] H. C. Liaw, B. Shirinzadeh, J. Smith, "Sliding-Mode Enhanced Adaptive Motion Tracking Control of Piezoelectric Actuation Systems for Micro/Nano Manipulation," IEEE Transactions on Control Systems Technology vol. 16, no. 4, pp. 826-833, 2008. Doi: 10.1109/TCST.2007.916301.

[70] Y. Gui, Q. Xu, F. Blaabjerg, H. Gong, "Sliding mode control with grid voltage modulated DPC for voltage source inverters under distorted grid voltage," CPSS Transactions on Power Electronics and Applications vol. 4, no. 3, pp. 244-254, 2019. Doi: 10.24295/CPSSTPEA.2019.00023.

[71] G. P. Incremona, M. Rubagotti, A. Ferrara, "Sliding Mode Control of Constrained Nonlinear Systems," IEEE Transactions on Automatic Control vol. 62, no. 6, pp. 2965-2972, 2017. Doi: 10.1109/TAC.2016.2605043.

[72] W. C. Wu, T. S. Liu, "Frequency-shaped sliding mode control for flying height of pickup head in near-field optical disk drives," IEEE Transactions on Magnetics vol. 41, no. 2, pp. 1061-1063, 2005. Doi: 10.1109/TMAG.2004.842020.

[73] H. Benbouhenni, Z. Boudjema, N. Bizon, P. Thounthong, N. Takorabet, "Direct Power Control Based on Modified Sliding Mode Controller for a Variable-Speed Multi-Rotor Wind Turbine System Using PWM Strategy," Energies vol. 15, pp. 3689, 2022. https://doi.org/10.3390/en15103689.

[74] B. Hu, H. Nian, J. Yang, M. Li, Y. Xu, "High-Frequency Resonance Analysis and Reshaping Control Strategy of DFIG System Based on DPC," In IEEE Transactions on Power Electronics vol. 36, no. 7, pp. 7810-7819, 2021. doi: 10.1109/TPEL.2020.3045860.

[75] R. M. Prasad, M. A. Mulla, "Rotor Position-Sensorless Algorithms for Direct Power Control of Rotor-Tied DFIG," In IEEE Transactions on Power Electronics vol. 3, no. 6, pp. 6213-6217, 2021. Doi: 10.1109/TPEL.2020.3040705.

[76] X. Lie, P. Cartwright, "Direct active and reactive power control of DFIG for wind energy generation," In IEEE Transactions on Energy Conversion vol. 21, no. 3, pp. 750-758, 2006. Doi: 10.1109/TEC.2006.875472.

[77] D. E. Kamel, M. Abdelkader, B. Larbi, P. M. Alex, B. Van Den, "A comprehensive review of LVRT capability and sliding mode control of grid-connected wind-turbine-driven doubly fed induction generator," Automatika vol. 57, no. 4, pp. 922-935, 2016. DOI: 10.7305/automatika.2017.05.1813.

[78] F. Amrane, A. Chaiba, "A novel direct power control for grid-connected doubly fed induction generator based on hybrid artificial intelligent control with space vector modulation," Rev. Roum. Sci. Techn.-Electrotechn. Et Energ. Vol. 61, no. 3, pp. 263-268, 2016.

[79] I. Yaichi, A. Semmah, P. Wira, Y. Djeriri, "Super-twisting sliding mode control of a doubly-fed induction generator based on the SVM strategy," Periodica Polytechnica Electrical Engineering and Computer Science vol. 63, no. 3, pp. 178–190, 2019.

[80] W. Ayrira, M. Ourahoua, B. El Hassounia, A. Haddi, "Direct torque control improvement of a variable speed DFIG based on a fuzzy inference system," Mathematics and Computers in Simulation vol. 167, pp. 308-324, 2020. https://doi.org/10.1016/j.matcom.2018.05.014.

[81] Z. Boudjema, A. Meroufel, Y. Djerriri, E. Bounadja, "Fuzzy sliding mode control of a doubly fed induction generator for energy conversion," Carpathian Journal of Electronic and Computer Engineering vol. 6, no. 2, pp. 7-14, 2013.

[82] A. Yahdou, B. Hemici, Z. Boudjema, "Second order sliding mode control of a dual-rotor wind turbine system by employing a matrix converter," Journal of Electrical Engineering vol. 16, no. 3, pp. 1-11, 2016.

[83] A. B. Moreira, T. A. D. S.Barros, V. S. D. C. Teixeira, R. R. D. Souza, M. V. D. Paula, E. R. Filho, "Control of Powers for Wind Power Generation and Grid Current Harmonics Filtering from Doubly Fed Induction Generator: Comparison of Two Strategies," In IEEE Access vol. 7, pp. 32703-32713, 2019. DOI: 10.1109/ACCESS.2019.2899456.

[84] E. Najib, D. Aziz, E. Abdelaziz, T. Mohammed, E. Youness, M. Khalid, B. Badre, "Direct torque control of doubly fed induction motor using three-level NPC inverter," Protection and Control of Modern Power Systems vol. 4, no. 17, pp. 1-9, 2019. https://doi.org/10.1186/s41601-019-0131-7.

[85] S. Mahfoud, A. Derouich, A. Iqbal, N. El Ouanjli, "Ant-Colony optimization-direct torque control for a doubly fed induction motor: An experimental validation," Energy Reports vol. 8, pp. 81-98, 2022. https://doi.org/10.1016/j.egyr.2021.11.239.

[86] Y. Quan, L. Hang, Y. He, Y. Zhang, "Multi-Resonant-Based Sliding Mode Control of DFIG-Based Wind System under Unbalanced and Harmonic Network Conditions," Appl. Sci. vol. 9, no. 6, pp. 1124, 2019. https://doi.org/10.3390/app9061124.

[87] G. Li, B. Chen, H. Chen, W. Deng, “Fractional-Order PIλDμ Controller Using Adaptive Neural Fuzzy Model for Course Control of Under actuated Ships.” Appl. Sci. vol. 12, no. 11, pp. 5604, 2022. https://doi.org/10.3390/app12115604.

[88] B. Habib, E. Bounadja, H. Gasmi, B. Nicu, C. Ilhami, "A new PD(1+PI) direct power controller for the variable-speed multi-rotor wind power system driven doubly-fed asynchronous generator”, Energy Reports vol. 8, pp. 15584-15594, 2022. https://doi.org/10.1016/j.egyr.2022.11.136.

[89] B. Habib, H. Gasmi, I. Colak, "Intelligent control scheme of asynchronous generator-based dual-rotor wind power system under different working conditions," Majlesi Journal of Energy Management vol. 11, no. 3, pp. 8-15, 2023.

[90] H. Benbouhenni, B. Nicu, T. Phatiphat, I. Colak, M. Pongsiri, "A new integral-synergetic controller for direct reactive and active powers control of a dual-rotor wind system," Measurement and Control vol. 57, no. 2, pp. 208-224, 2024. Doi: 10.1177/00202940231195117.

[91] B. Habib, H. Gasmi, I. Colak, B. Nicu, T. Phatiphat, "Synergetic-PI controller based on genetic algorithm for DPC-PWM strategy of a multi-rotor wind power system," Scientific Report vol. 13, pp. 13570, 2023. https://doi.org/10.1038/s41598-023-40870-7.

[92] B. Habib, N. Bizon, I. Colak, "Super-twisting hysteresis controller for multi-rotor wind energy systems," Int’l Journal of Electronics vol. 112, no. 3, pp. 453–472, 2024. DOI: 10.1080/00207217.2024.2312086.

[93] H. Benbouhenni, I. Colak, N. Bizon, "Backstepping control for multi-rotor wind power systems," Majlesi Journal of Energy Management vol. 11, no. 4, pp. 8-15, 2023.

[94] B. Habib, D. Zellouma, N. Bizon, I. Colak, "A new PI (1 +PI) controller to mitigate power ripples of a variable-speed dual-rotor wind power system using direct power control," Energy Reports vol. 10, pp. 3580-3598, 2023. Doi: 10.1016/j.egyr.2023.10.007.

[95] B. Habib, I. Colak, N. Bizon, A. G. Mazare, T. Phatiphat, "Direct Vector Control Using Feedback PI Controllers of a DPAG Supplied by a Two-Level PWM Inverter for a Multi-rotor Wind Turbine System," Arabian Journal for Science and Engineering vol. 48, pp. 15177–15193, 2023. Doi: 10.1007/s13369-023-08035-w.